

**An-Najah National University**

**Faculty of Graduate studies**

**Structural, electronic, magnetic & elastic properties of  
Full-Heusler alloys: normal and inverse  $Zr_2RhGa$ ,  
 $Co_2TiSn$  using FP-LAPW method**

**By**

**Doha Naser Abu Baker**

**Supervisor**

**Prof. Mohammed Abu-Jafar**

**This Thesis is Submitted in Partial Ful fillment of the Requirements  
for the Degree of Master of Physics, Faculty of Graduated Studies,  
An-Najah National University, Nablus - Palestine.**

**2018**

**Structural, electronic, magnetic & elastic properties of  
Full-Heusler alloys: normal and inverse  $Zr_2RhGa$ ,  
 $Co_2TiSn$  using FP-LAPW method**

**By**

**Doha Naser Abu Baker**

**This thesis was defended successfully on 24 /10/2018 and approved by:**

**Defense committee members:**

**Signature**

- **Prof. Mohammed Abu-Jafar / Supervisor** .....
- **Prof. Jihad Asad / External Examiner** .....
- **Prof. Mohammed El-Saeed / Internal Examiner** .....

## **Dedication**

To my kind parents, who are impossible to be thanked adequately for everything they have done for me and my future and learn me to be ambitious person. They are really the best model for perfect parents and they are the main cause of success in my life. ALLAH bless them. To my beloved husband (Hasan), who shares me all moments and helps me to overcome difficulties to continue moving forward. He also provides me encouragement, motivation and support to achieve my ambitions successfully.

To my lovely sister (Saja) and my lovely brothers (Thaer, Fadi & Rami), who always encourage me and give me a powerful support. They are always present to help and motivate me .To my cute babies (Sara & Saeed).

## **Acknowledgments**

All thanks to Allah, who gives me health, patience and knowledge to complete my thesis. I would like to express sincere thanks to my advisor and instructor Dr. Mohammed Abu-Jafar for his guidance, assistance, supervision and contribution of valuable suggestions, I would like to thank Ms. Nisreen Hamadneh who helps me to use some programs. Never forget my faculty members of physics department for their help and encouragement. Finally, special thanks to my friends for their moral support and cares.

## الإقرار

أنا الموقعة أدناه، مقدمة الرسالة التي تحمل عنوان:

### **Dyslipidemia in young patients with type I diabetes mellitus in Nablus city: a cross-sectional study**

أقر بأن ما اشتملت عليه هذه الرسالة هي من نتائج جهدي الخاص، باستثناء ما تمت الإشارة إليه حيثما ورد، وأن هذه الرسالة ككل أو أي جزء منها لم يقدم من قبل لنيل درجة أو لقب علمي أو بحثي لدى أي مؤسسة تعليمية أو بحثية أخرى.

## **Declaration**

The work provided in this thesis unless otherwise referenced, is the researcher's own work, and has not been submitted elsewhere for any other degree or qualification.

**Student's name:**

اسم الطالبة:

**Signature:**

التوقيع:

**Date:**

التاريخ:

## Table of contents

No.	Content	Page
	Dedication	<b>Iii</b>
	Acknowledgment	<b>Iv</b>
	Declaration	<b>V</b>
	List of Tables	<b>Vii</b>
	List of Figures	<b>Viii</b>
	Abstract	<b>X</b>
1	<b>Chapter One: Introduction</b>	<b>1</b>
2	<b>Chapter Two: Methodology</b>	<b>5</b>
2.1	The Open-Heimer Approximation	<b>5</b>
2.2	Hartree and Hartree-Fock Approximation	<b>6</b>
2.3	Density Functional Theory	<b>6</b>
2.4	Single Particle Kohn-Sham Equation	<b>7</b>
2.5	The Exchange-Correlation Functional	<b>9</b>
2.6	Local Density Approximation(LDA)	<b>10</b>
2.7	Generalized Gradient Approximation(GGA)	<b>11</b>
2.8	Augmented Plane Wave (APW) Method.	<b>12</b>
2.9	The Linearized Augmented Plane Wave (LAPW) Method.	<b>13</b>
2.10	The Augmented Plane Wave+Local Orbits (LAPW+Lo) Method	<b>14</b>
3	<b>Chapter Three: Results and Discussion</b>	<b>16</b>
3.1	Computational Method	<b>16</b>
3.2	Structural Properties	<b>17</b>
3.3	Magnetic Properties	<b>22</b>
3.4	Electronic Properties	<b>23</b>
3.5	Elastic Properties	<b>38</b>
4	<b>Chapter Four: Conclusion</b>	<b>43</b>
	References	<b>45</b>
	المخلص	<b>b</b>

**List of Tables**

<b>No.</b>	<b>Table captions</b>	<b>Page</b>
<b>1</b>	Calculated lattice parameter, bulk modulus, pressure derivative for normal Heusler $\text{Co}_2\text{TiSn}$ and inverse Heusler $\text{Zr}_2\text{RhGa}$ compounds.	<b>21</b>
<b>2</b>	Total magnetic moment for normal and inverse Heusler $\text{Co}_2\text{TiSn}$ Compound.	<b>22</b>
<b>3</b>	Total magnetic moment for normal and inverse Heusler $\text{Zr}_2\text{RhGa}$ Compound.	<b>22</b>
<b>4</b>	Energy band gaps for normal Heusler $\text{Co}_2\text{TiSn}$ and normal Heusler $\text{Zr}_2\text{RhGa}$ Compounds.	<b>28</b>
<b>5</b>	Energy band gaps for inverse Heusler $\text{Co}_2\text{TiSn}$ and inverse Heusler $\text{Zr}_2\text{RhGa}$ Compounds.	<b>29</b>
<b>6</b>	Elastic constants for normal Heusler $\text{Co}_2\text{TiSn}$ and inverse Heusler $\text{Zr}_2\text{RhGa}$ Compounds.	<b>40</b>

## List of Figures

No.	Figure captions	Page
<b>1</b>	Flowchart for the $n^{th}$ iteration in the self-consistent procedure to solve Hartree-Fock or Kohn-Sham equations.	<b>9</b>
<b>2</b>	Scheme of Augmented Plane Wave.	<b>12</b>
<b>3</b>	The crystal structure of (a) normal Heusler $\text{Co}_2\text{TiSn}$ (b) inverse Heusler $\text{Co}_2\text{TiSn}$ (c) normal Heusler $\text{Zr}_2\text{RhGa}$ (d) inverse Heusler $\text{Zr}_2\text{RhGa}$ compounds.	<b>18</b>
<b>4</b>	Total energy as function of the volume for (a) normal $\text{Co}_2\text{TiSn}$ (b) normal $\text{Zr}_2\text{RhGa}$ and (c) inverse $\text{Zr}_2\text{RhGa}$ (d) inverse $\text{Co}_2\text{TiSn}$ compounds on unit cell of volume.	<b>19</b>
<b>5</b>	Band structure spin up by using PBE-GGA method for (a) normal $\text{Co}_2\text{TiSn}$ (b) inverse $\text{Co}_2\text{TiSn}$ (c) inverse $\text{Zr}_2\text{RhGa}$ compounds.	<b>25</b>
<b>6</b>	Band structure spin down by using PBE-GGA method for (a) normal $\text{Co}_2\text{TiSn}$ (b) inverse $\text{Co}_2\text{TiSn}$ (c) inverse $\text{Zr}_2\text{RhGa}$ compounds	<b>26</b>
<b>7</b>	Band structure by using PBE-GGA method for normal $\text{Zr}_2\text{RhGa}$ compound.	<b>27</b>
<b>8</b>	Band structure spin up by using mBJ-GGA method (a) normal $\text{Co}_2\text{TiSn}$ (b) inverse $\text{Zr}_2\text{RhGa}$ compounds .	<b>27</b>
<b>9</b>	Band structure spin down by using mBJ-GGA method (a) normal $\text{Co}_2\text{TiSn}$ (b) inverse $\text{Zr}_2\text{RhGa}$ compounds .	<b>28</b>
<b>10</b>	(a) Total density of states of spin up for normal $\text{Co}_2\text{TiSn}$ and partial density of states of spin up for (b) Co atom (c) Ti atom (d) Sn atom of normal $\text{Co}_2\text{TiSn}$ compound.	<b>31</b>
<b>11</b>	(a) Total density of states of spin down for normal $\text{Co}_2\text{TiSn}$ and partial density of states of spin up for (b) Co atom (c) Ti atom (d) Sn atom of normal $\text{Co}_2\text{TiSn}$ compound.	<b>32</b>
<b>12</b>	(a) Total density of states for normal $\text{Zr}_2\text{RhGa}$ and partial density of states for (b) Zr atom (c) Rh atom (d) Ga atom of normal $\text{Zr}_2\text{RhGa}$ compound.	<b>33</b>
<b>13</b>	(a) Total density of states of spin up for inverse $\text{Co}_2\text{TiSn}$ and partial density of states of spin down for (b) Co atom (c) Ti atom (d) Sn atom of inverse $\text{Co}_2\text{TiSn}$ compound.	<b>34</b>
<b>14</b>	(a) Total density of states of spin down for inverse $\text{Co}_2\text{TiSn}$ and partial density of states of spin down for (b) Co atom (c) Ti atom (d) Sn atom of inverse $\text{Co}_2\text{TiSn}$ compound.	<b>35</b>

<b>15</b>	(a) Total density of states of spin up for inverse $Zr_2RhGa$ and partial density of states of spin up for (b) Zr atom (c) Rh atom (d) Ga atom of inverse $Zr_2RhGa$ compound.	<b>36</b>
<b>16</b>	(a) Total density of states of spin down for inverse $Zr_2RhGa$ and partial density of states of spin down for (b) Zr atom (c) Rh atom (d) Ga atom of inverse $Zr_2RhGa$ compound.	<b>37</b>

**Structural, electronic, magnetic & elastic properties of Full-Heusler alloys: normal and inverse  $Zr_2RhGa$ ,  $Co_2TiSn$  using FP-LAPW method**

**By**

**Doha Naser Abu Baker**

**Supervisor**

**Prof. Mohammed Abu-Jafar**

**Abstract**

The equilibrium structural parameters, electronic, magnetic and elastic properties of the normal and inverse  $Zr_2RhGa$  and  $Co_2TiSn$  Full-Heusler compounds have been studied using density functional theory (DFT) and full-potential linearized augmented plane wave (FP-LAPW) method as implemented in the WIEN2k package. The Generalized Gradient Approximation (GGA) has been used for the exchange-correlation potential ( $V_{xc}$ ) to compute the equilibrium structural parameters; lattice constant ( $a$ ), bulk modulus ( $B$ ), bulk modulus pressure derivative ( $B'$ ). In addition to GGA approach, the modified Becke Johnson (mBJ) scheme has been used to calculate the band gap energies. The normal Heusler  $Co_2TiSn$  compound and inverse Heusler  $Zr_2RhGa$  compound within GGA and mBJ approaches are found to have a half-metallic behavior, with an indirect energy gap in the spin down configuration. The total magnetic moment for normal  $Co_2TiSn$  and inverse  $Zr_2RhGa$  Full-Heusler compounds are to some extent compatible with the experimental and theoretical results. The normal  $Co_2TiSn$  and inverse  $Zr_2RhGa$  Full-Heusler compounds are mechanically stable; are satisfy the Born mechanical stability criteria.  $B/S$  ratio shows that the normal  $Co_2TiSn$  has a brittle nature. While the inverse has a ductile

nature. Poisson's ratio ( $\nu$ ) values show that the normal  $\text{Co}_2\text{TiSn}$  and inverse  $\text{Zr}_2\text{RhGa}$  Full-Heusler compounds have an ionic bond nature.

# Chapter One

## Introduction

In recent years, Heusler alloys received growing attention due to their interesting physical properties [1-4], especially the half-metallic (HM) character, half-metallic (HM) materials exhibiting a 100% spin polarization around the Fermi surface [1-3] (a half metal is a ferromagnetic with a gap in one of the spin directions at the Fermi energy  $\epsilon_f$ ). Half metals can be used as spin injectors for magnetic random access memories and other spin dependent devices [2].

A lot of alloys were predicted to be half-metallic (HM) materials. In fact, investigating and searching for new (HM) materials are mainly focusing on the Heusler alloys [3-17].

From structural point of view, Heusler family can be described by two variants: Full Heusler  $X_2YZ$  phases, which typically crystallize in  $Cu_2MnAl(L21)$ -type structure and the Half-Heusler  $XYZ$  which typically crystallize in  $NiMnSb (C1b)$  type structure, X and Y transition elements are 3d, 4d or 5d elements and Z is s-p elements.

The Full-Heusler compounds are divided into two types: normal Heusler and inverse Heusler.

The atoms in normal Heusler compounds are lined up in  $X_2: (1/4, 1/4, 1/4), (3/4, 3/4, 3/4), Y(1/2, 1/2, 1/2),$  and  $Z(0, 0, 0),$  and the atoms in inverse

Heusler compounds are lined up in  $X_2:(1/4,1/4,1/4)$ ,  $(1/2,1/2,1/2)$ ,  $Y(3/4,3/4,3/4)$ , and  $Z(0,0,0)$  [18].

There are a lot of previous studies that have been done on Heusler compounds and other compounds (half-metallic compounds) by using different methods [19-24].

In 2006, Kandpal et al. [19] measured the lattice parameter and the total magnetic moment for inverse Heusler  $Co_2TiSn$  compound and found to be  $7.072 \text{ \AA}^0$ ,  $2 \mu_B$ , respectively. Also, the magnetic moment was calculated using LMTO-ASA code [20], SPRKKR code [21], FP-LAPW method [22] and FPLMTO method [23], it is found to be  $1.40 \mu_B$ ,  $1.55 \mu_B$ ,  $2 \mu_B$ ,  $2 \mu_B$ , respectively. It is clear that the LMTO-ASA and SPRKKR codes fail to get the correct measured total magnetic moment, while Wien2k and FPLMTO codes do correctly obtain minority gap in this compound and also measured correctly the magnetic moment  $2 \mu_B$  per formula unit.

In 2014, Birsan and Kuncser [24] studied the electronic, structural and magnetic properties of  $Zr_2CoSn$  Full-Heusler compound by using FP-LAPW method. They calculated the energy band gap ( $E_g = 0.543 \text{ eV}$ ), total magnetic moment ( $M_{tot} = 3 \mu_B$ ) and the lattice parameter ( $a = 6.76 \text{ \AA}^0$ ). In 2014, A. Birsan [25] investigated structural and magnetic properties of the Full-Heusler compound,  $Zr_2CoAl$  using FP-LAPW method. He calculated the lattice parameter ( $a = 6.54 \text{ \AA}^0$ ), energy band gap ( $E_g = 0.48 \text{ eV}$ ), and total magnetic moment ( $M_{tot} = 2 \mu_B$ ).

In 2015, Wang et al. [26] studied the half-metallic state and magnetic properties versus the lattice constant in  $Zr_2RhZ$  ( $Z = Al, Ga, In$ ) Heusler alloys by using CASTEP code. The CASTEP code is based on the density functional theory (DFT) pseudo-potential method [27,28]. The calculated lattice parameters were found to be 6.66, 6.64 and 6.81  $\text{\AA}$ , respectively and magnetic moment for all alloys was found to be  $2 \mu_B$  [26].

In 2017, Jain et al. [29] studied electronic structure, magnetic and optical properties of  $Co_2TiZ$  ( $Z = B, Al, Ga, In$ ) Heusler alloys by using FP-LAPW code. They found the lattice parameters to be 5.494, 5.842, 5.845 and 6.087  $\text{\AA}$ , respectively. Bulk modulus is found to be 233, 182, 184 and 161 GPa, respectively. Energy band gap is found to be 0.1, 0.44, 0.16 and 0.06 eV, respectively, and total magnetic moment is found to be 1, 0.99, 1 and 1.03  $\mu_B$ , respectively.

In 2017, Weia et al. [30] estimated the electronic, Fermi surface, Curie temperature and optical properties of  $Zr_2CoAl$  compound by using FPLO code [31,32]. They calculated the lattice parameter ( $a = 6.629 \text{\AA}$ ), Bulk modulus ( $B = 106.8 \text{ GPa}$ ), and the total magnetic moment ( $M_{tot} = 2 \mu_B$ ) for the normal Full-Heusler structure ( $Cu_2MnAl$ ).

In present work, the motivation is to investigate electronic, structural, magnetic and elastic properties of normal Heusler  $Co_2TiSn$  and inverse Heusler  $Zr_2RhGa$  compounds by using the full potential-linearized augmented plane wave method [FP-LAPW method] within the Perdew-

Burke-Ernzerhof generalized gradient approximation [PBE-GGA] [33] integrated in Wien2k code [22].

In chapter two, presents methodology details. In chapter three, we report and discuss our obtained results for the system of interest, Finally Conclusions are summarized in chapter four.

## Chapter Two

### Methodology

Schrodinger equation; given in Equation 1 below; is very hard to be solved for a N-body system. It has become evident that we must involve some approximations to face a lot of problems of the body [22].

$$\hat{H} = \frac{-\hbar^2}{2} \sum_i \frac{\nabla_{R_i}^2}{M_i} - \frac{\hbar^2}{2} \sum_i \frac{\nabla_{r_i}^2}{m_e} - \frac{1}{4\pi\epsilon_0} \sum_{i,j} \frac{e^2 Z_i}{|R_i - \vec{r}_j|} + \frac{1}{8\pi\epsilon_0} \sum_{i \neq j} \frac{e^2}{|\vec{r}_i - \vec{r}_j|} + \frac{1}{8\pi\epsilon_0} \sum_{i \neq j} \frac{e^2 Z_i Z_j}{|R_i - R_j|} \quad (1)$$

The first term is the kinetic energy operator for the nuclei ( $T_n$ ), the second term is for the kinetic energy of electrons ( $T_e$ ) and the last three terms describe the coulomb interaction between the electron and the nuclei ( $V_{en}$ ), between the electron and other electrons ( $V_{ee}$ ), and between the nuclei and other nuclei ( $V_{nn}$ ).

There isn't an exact solution to this Schrodinger equation. However, to solve this problem, there are some approximations.

The approximations are as follows:

#### 2.1 The Open-Heimer Approximation

This approximation assumes that the nuclei are more massive than electrons, and then  $T_n = \text{zero}$  and  $V_{nn} = \text{constant}$  then  $\mathbf{H} = \mathbf{T}_e + \mathbf{V}_{ee} + \mathbf{V}_{ext}$  (2)

Where the External Potential is given by  $\mathbf{V}_{ext} = (\mathbf{V}_{nn} + \mathbf{V}_{en})$

## 2.2 Hartree and Hartree-Fock Approximation

Hartree approximation depends on the principle of pauli exclusion. This means that no two electrons can have the same set of quantum numbers.

In Hartree-Fock Approximation, many system particles have been solved by assuming that the electrons are independent and separated from each other. Thus, the wave function of electrons can be written as:

$$\Psi(\mathbf{r}_1, \mathbf{r}_2, \mathbf{r}_3, \dots, \mathbf{r}_N) = \Psi_1(\mathbf{r}_1) \Psi_2(\mathbf{r}_2) \Psi_3(\mathbf{r}_3) \dots \Psi_N(\mathbf{r}_N) \quad (3)$$

The  $\Psi_n(\mathbf{r}_n)$  is the wave function for the electrons, and so the total Hamiltonian can be written as:

$$(T_s + V_{ext} + V_H) \Psi(\mathbf{r}) = E \Psi(\mathbf{r}) \quad (4)$$

The  $T_s$  is the kinetic energy and  $V_{ext}$  is the external potential whereas the  $V_H$  is the Hartree potential for non-interacting electrons, and it can be written as:

$$V_H = \frac{1}{8\pi\epsilon_0} \sum_{ij} \frac{|\psi(\mathbf{r}_i)|^2 |\psi(\mathbf{r}_j)|^2 d^3\mathbf{r}_i d^3\mathbf{r}_j}{|\vec{\mathbf{r}}_i - \vec{\mathbf{r}}_j|} \quad (5)$$

## 2.3 Density Functional Theory (DFT)

DFT provides a way to solve many body problem into a single body problem, its successful minimizing of the energy functional will produce the ground state density  $\rho_0$ .

So  $E(\rho)$  is rewritten as the Hartree total energy plus another smaller unknown functional called exchange-correlation functional,  $E_{xc}(\rho)$ .

$$\mathbf{E}(\boldsymbol{\rho}) = \mathbf{T}_s(\boldsymbol{\rho}) + \mathbf{E}_c(\boldsymbol{\rho}) + \mathbf{E}_H(\boldsymbol{\rho}) + \mathbf{E}_{ii}(\boldsymbol{\rho}) + \mathbf{E}_{xc}(\boldsymbol{\rho}) \quad (6)$$

Whereas  $T_s$  is single kinetic energy,  $E_c$  is coloumb energy between nuclei and electrons.  $E_{ii}(\rho)$  represents the interaction between the nuclei.  $E_{xc}$  is found to be the exchange correlation energy and it is unknown part, while  $E_H$  is Hartree potential.

$$\mathbf{E}_H(\boldsymbol{\rho}) = \frac{e^2}{2} \int \mathbf{d}^3\mathbf{r} \mathbf{d}^3\mathbf{r}' \frac{\boldsymbol{\rho}(\mathbf{r})\boldsymbol{\rho}(\mathbf{r}')}{|\mathbf{r}-\mathbf{r}'|} \quad (7)$$

Based on the variational principle, a set of effective one-particle Schrodinger equation (Kohn-Sham Equation) is given as:

$$[\mathbf{T}_s + \mathbf{V}_{\text{ext}}(\mathbf{r}) + \mathbf{V}_H(\boldsymbol{\rho}(\mathbf{r})) + \mathbf{V}_{xc}(\boldsymbol{\rho}(\mathbf{r}))]\Phi_i(\mathbf{r}) = \varepsilon_i\Phi_i(\mathbf{r}) \quad (8)$$

Where  $\varepsilon_i$  is the single particle energy,  $\Phi_i$  is the electron wave function,  $V_H$  is the Hartree potential,  $V_{\text{ext}}$  is the coulomb potential and  $V_{xc}$  is the exchange-correlation potential.

## 2.4 Single Particle Kohn-Sham Equation.

The LAPW method is a procedure to solve the Kohn-Sham equations of the ground state density, total energy and (Kohn-Sham) eigenvalues (energy bands) of a many electrons system. In such method, we can interpret Equation 7 as the energy function of a *non-interacting* classical electron gas, subject to two external potentials: one is due to the nuclei  $\hat{V}_{\text{ext}}[\rho]$ , while the other is due to the exchange correlation effects  $\hat{V}_{xc}[\rho]$ . The corresponding Hamiltonian is called the Kohn-Sham Hamiltonian. The exact ground-state density  $\rho(\vec{r})$  of an N-electron system is given as:

$$\rho(\vec{r}) = \sum_{i=1}^N \Phi_i^*(\vec{r}) \Phi_i(\vec{r}) = \sum_{i=1}^N |\Phi_i(\vec{r})|^2 \quad (9)$$

Where the single-particle wave functions  $\Phi_i(\vec{r})$  are the N lowest-energy solutions of the Kohn- Sham equation

$$\widehat{H}_{KS} \Phi_i = \epsilon_i \Phi_i \quad (10)$$

In certain occasions, Kohn-Sham equation is written as:

$$\widehat{H} \Phi_i(\vec{r}) = \left[ -\frac{\hbar^2}{2m_e} \nabla_i^2 + V_{eff} \right] \Phi_i = \epsilon_i \Phi_i \quad (11)$$

Where  $\widehat{H}$  is known to be the Hamiltonian operator, the effective potential  $V_{eff}(\vec{r})$  is the sum of the external, Hartree (electrostatic), and the exchange correlation potential.  $V_{eff}(\vec{r})$  is stated as:

$$V_{eff}(\vec{r}) = V_{ext}(\vec{r}) + \frac{\delta E_H[\rho]}{\delta \rho} + \frac{\delta E_{xc}[\rho]}{\delta \rho} = V_{ext}(\vec{r}) + V_H + V_{xc}(\vec{r}) \quad (12)$$

$$\text{Where } V_H = \frac{e^2}{4\pi\epsilon_0} \int \frac{\rho(\vec{r}')}{|\vec{r} - \vec{r}'|} d\vec{r}'$$

It is shown from eqn. (12) that  $V_H$  and  $V_{xc}$  depend on the charge density  $\rho(\vec{r})$ , which in turn depends on the  $\Phi_i$ . This means that a self-consistency problem occurs and therefore needs to be dealt with the solution  $\Phi_i$ . The solution  $\Phi_i$  determines the original equation ( $V_H$  and  $V_{xc}$  in  $H_{KS}$ ), and the equation cannot be written down and solved before its solution is being recognized. Some starting density  $\rho_0$  is guessed, and a Hamiltonian  $H_{KS1}$  can be constructed with it. The eigenvalue problem is also solved, and  $\Phi_1$  can be determined by  $\rho_1$ . And now  $\rho_1$  can be used to construct  $H_{KS2}$  which will yield  $\rho_2$ , etc. The procedure can be subsequently used as long as the series convergence and  $\rho_f$  get out.

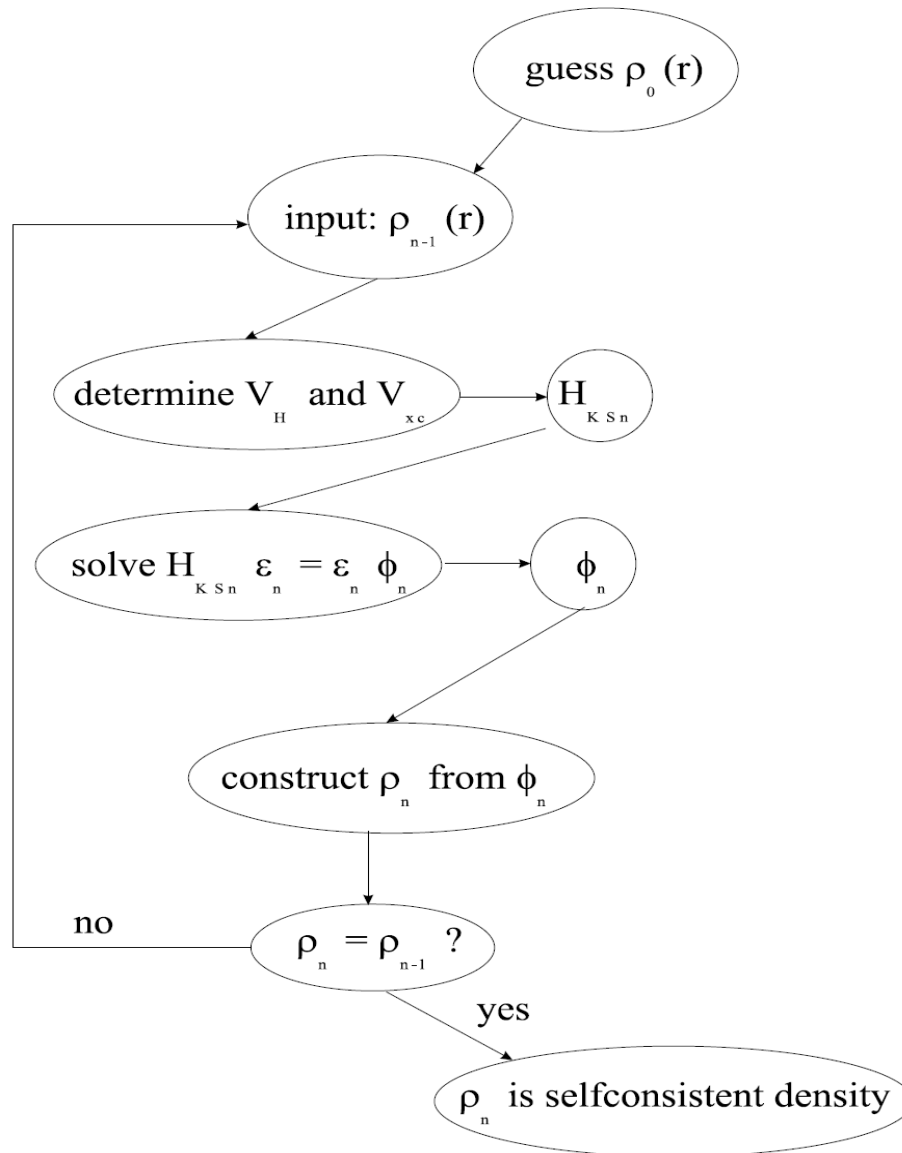


**Figure 1:** Flowchart for the  $n^{\text{th}}$  iteration in the self-consistent procedure to solve Hartree-Fock or Kohn-Sham equations.

## 2.5 The Exchange-Correlation Functional.

The Kohn-Sham scheme described above was accurate: apart from the preceding Born-Oppenheimer approximation, no other approximations were made. But the fact that we do not know the exchange-correlation functional was neglected so far and is still made unknown.

Consequently, the introduction of an approximation is needed. The two often - used approximations are LDA (Local Density Approximation) and GGA (Generalized Gradient Approximation).

## 2.6 Local Density Approximation (LDA).

A widely used approximation-called (LDA) – is to postulate that the exchange-correlation functional has the following form:

$$E_{xc}^{LDA} = \int \rho(\vec{r}) \varepsilon_{xc}[\rho(\vec{r})] d\vec{r} \quad (13)$$

Where  $\varepsilon_{xc}[\rho(\vec{r})]$  is the exchange-correlation energy per particle of a uniform (a homogeneous) electron gas, it only depends on the electron density  $\rho(\vec{r})$ , thus the name given is the “local density approximation”.

The exchange-correlation energy due to a particular density could be found by dividing the material into infinitesimally small volumes with a constant density [17].

Each volume contributes to the total exchange correlation energy by an amount equal to the exchange correlation energy of an identical volume and filled with a homogeneous electron gas. The exchange-correlation energy is decomposed into exchange and correlation terms linearly as shown below:

$$E_{xc}^{LDA} = E_x^{LDA} + E_c^{LDA} \quad (14)$$

The first contribution is the exchange energy that comes from the Pauli Exclusion Principle. The second contribution, called the correlation energy  $E_c^{LDA}$ , originates from the interaction of electrons having the same spin [18].

The next logical step to improve the LDA is to make the exchange-correlation contribute to every infinitesimal volume not only to be dependent on the local density in that volume, but also to contribute to the density in the neighboring volumes. To sum up, the gradient of the density will play a role. This approximation is called the Generalized Gradient Approximation (GGA).

## 2.7 Generalized Gradient Approximation (GGA).

Where as LDA uses the exchange energy density of the uniform electron gas, regardless of the homogeneity of the real charge density, the GGA is concerned with such inhomogeneities (non-uniform charge density) by including the gradient of the electron density in the functional. The GGA uses the gradient of the charge density  $\vec{\nabla}\rho(\vec{r})$ .

The GGA can be conveniently written as follows

$$E_{xc}^{GGA} = \int \rho(\vec{r}) \varepsilon_{xc}[\rho(\vec{r}), \vec{\nabla}\rho(\vec{r})] d\vec{r} \quad (15)$$

GGA seeks to improve the accuracy of the local density approximation

## 2.8 Augmented Plane Wave (APW) Method.

Augmented plane wave method is introduced by Slater as a basis of functions for solving the one-electron equation. APW method is a procedure for solving the Kohn-Sham equation. In the APW scheme, the unit cell is divided into two types of regions: (I) atomic centered muffin-tin (MT) spheres with radius  $R_\alpha$ , and (II) the remaining interstitial region as shown in figure 2.

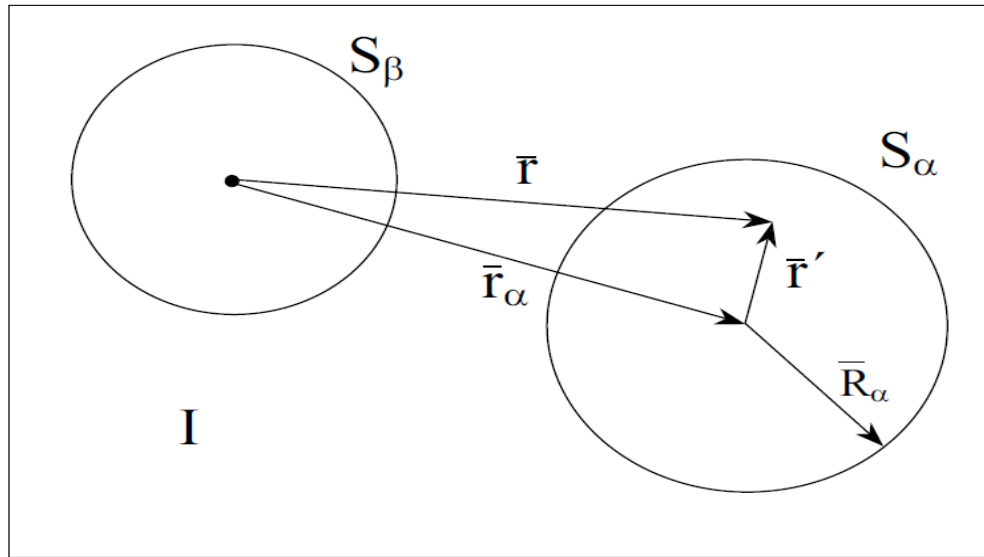


**Figure 2:** Scheme of Augmented Plane Wave.

In both types of regions, different basis sets are used. In the region far away from the nuclei, electrons are almost free, so plane waves are employed. However, close to the nuclei, the electrons behave almost as if they were in a free atom and therefore they can be described as atomic like- wave functions (radial solution of Schrödinger's equation)

The introduction of such a basis is due to the fact that close to the nuclei the potential and wave functions are very similar to those in an atom, while

they appear to be smoother between the atoms. In other words, the further the region from the nuclei, the more or less “free” the electrons would become.

The APWs consists of:

$$\Phi_{\vec{K}}^{\vec{k}}(\vec{r}, \mathbf{E}) = \begin{cases} \frac{1}{\sqrt{V}} e^{i(\vec{k}+\vec{K})\cdot\vec{r}}, & \vec{r} \in \mathbf{I} \\ \sum_{l,m} A_{lm}^{\alpha, \vec{k}+\vec{K}} u_l^\alpha(r', \mathbf{E}) Y_m^l(\hat{r}'), & \vec{r}' < S_\alpha \end{cases} \quad (16)$$

Where  $\vec{K}$  is the reciprocal lattice vectors and  $\vec{k}$  is the wave vector inside the Brillion zone,  $V$  is the volume of the unit cell,  $\vec{r}'$  is the poison vector inside the sphere  $S_\alpha$ ,  $u_l^\alpha$  is the numerical solution to the radial Schrodinger equation at the energy  $\varepsilon$ .

## 2.9 The linearized Augmented Plane Wave (LAPW) Method.

The linearized augmented plane wave method (LAPW) scheme was introduced by Andersen [ref.] who suggested the expansion of the energy dependence on radial wave functions  $u(r')$  inside the atomic spheres with its energy derivative  $\frac{\partial u^\alpha(r', E)}{\partial E} = \dot{u}^\alpha(r', E)$ . In this scheme, a linear combination of radial function times spherical harmonics are used.

Inside the atomic sphere of radius  $R_t$  a linear combination of the radial functions times spherical harmonics  $Y_{lm}(r)$  is used, where  $u_l(r, E_l)$  - at the origin - is the regular solution of the radial Schrödinger equation for energy  $E_l$  and the spherical part of the potential inside the atomic sphere  $\dot{u}^\alpha(r', E)$  is the energy derivative of  $u_l$  taken at the same energy  $E_l$

$$\phi_{\vec{K}}^{\vec{k}}(\vec{r}, E) = \sum_{l,m} (a_{lm}^{\alpha, \vec{k}+\vec{K}} u_l^\alpha(r', E) + b_{lm}^{\alpha, \vec{k}+\vec{K}} \dot{u}_l^\alpha(r', E)) Y_m^l(\hat{r}'), \quad r' < R_\alpha \quad (17)$$

In the interstitial region, a plane wave expansion is used.

$$\phi_{\vec{K}}^{\vec{k}}(\vec{r}, E) = \frac{1}{\sqrt{V}} e^{i(\vec{k}+\vec{K}) \cdot \vec{r}}, \quad \vec{r} \in I \quad (18)$$

## 2.10 The Augmented Plane Wave + Local Orbits (LAPW+Lo) Method.

This alternative approach was proposed by Sjöstedt et al [18], namely the APW+lo (local orbital) method. They have shown that the standard LAPW method with the additional constraint on the PWs of matching in value and slope to the solution inside the sphere is not the most efficient way to linearize Slater's APW method. It can be made much more efficient when one uses the standard APW basis, but, in fact, with  $u_l(r, E_1)$  at a fixed energy  $E_1$  in order to keep the linear eigen value problem. One then adds a new local orbital (lo) to have enough variation flexibility in the radial basis functions [19]:

$$\Phi_{\vec{k}_n}^{\vec{k}_n} = \sum_{lm} [a_{lm}^{\vec{k}_n} u_l(r, E_1)] Y_{lm}(\hat{r}) \quad (19)$$

$$\Phi_{lm}^{\text{lo}} = \begin{cases} 0, & \vec{r} \in I \\ [a_{lm}^{\text{lo}} u(r', E_{1,l}) + b_{lm}^{\text{lo}} \dot{u}_l(r', E_{1,l})] Y_{lm}(\hat{r}), & r' < R_\alpha \end{cases} \quad (20)$$

The coefficient  $a_{lm}^{lo}$ ,  $b_{lm}^{lo}$  are decided by necessities that  $\phi_{lm}^{lo}$  should be regularized and has a zero value with a slope at the sphere border.

In its general form, the LAPW method expands the potential in the following form:

$$V(\vec{r}) = \begin{cases} \sum_{lm} V_{lm}(\mathbf{r}) Y_{lm}(\hat{\mathbf{r}}), & \text{inside sphere} \\ \sum_{\vec{k}} V_{\vec{k}} e^{i\vec{k} \cdot \vec{r}}, & \text{outside sphere} \end{cases} \quad (21)$$

## Chapter Three

### Results and Discussion

#### 3.1 Computational Method

In this work, First-principles full-potential linearized augmented plane wave [FP-LAPW] computations have been performed as implemented in Wien2k package [22] within the generalized gradient approximation [PBE-GGA] [33]. For the compound  $\text{Co}_2\text{TiSn}$ , the muffin-tin radii ( $R_{\text{MT}}$ ) of Co, Ti and Sn atoms are 2.22, 2.17 and 2.22 a.u., respectively and for the compound  $\text{Zr}_2\text{RhGa}$ ,  $R_{\text{MT}}$  of Zr, Rh and Ga atoms are 2.37, 2.49 and 2.37 a.u., respectively.

The number of plane waves was restricted by  $K_{\text{MAX}} R_{\text{MT}} = 8$  and the expansions of the wave functions was set to  $l=10$  inside the muffin tin spheres. 35k points in the irreducible Brillion zone (BZ) with grid  $10 \times 10 \times 10$  Monkhorst-Pack (MP) [34] meshes (equivalent to 1000k points in the full Brillion zone (BZ)) are used to obtain self-consistency for  $\text{Co}_2\text{TiSn}$  and  $\text{Zr}_2\text{RhGa}$  compounds.

The self-consistent calculations are considered to converge only when the calculated total energy of the crystal converges to less than  $10^{-5}$  Ry. The elastic component  $C_{11}$ ,  $C_{12}$  and  $C_{44}$  are calculated by using the method developed by Morteza Jamal [35] and integrated in Wien2k code as the IRelast package. The elastic constants of the cubic phase are calculated by using second-order derivative within formalism of the Wien2k code.

### 3.2 Structural Properties

The optimized lattice constant (a), bulk modulus (B), and its pressure derivative (B') were calculated by fitting the total energy to Murnaghan's equation of state (EOS) [36]. Murnaghan's equation of state (EOS) is given by:

$$E(V) = E_0 + \frac{BV}{B'} \left[ \frac{(V_0/V)^{B'}}{B' - 1} + 1 \right] - \frac{B}{B' - 1} V_0 \quad (22)$$

Where  $E_0$  is the minimum energy, B is the bulk modulus at the equilibrium volume and B' is the pressure derivative of the bulk modulus at the equilibrium volume.

$$\text{Pressure, } P = -\frac{dE}{dV}, \text{ Bulk modulus, } B = -V \frac{dP}{dV} = V \frac{d^2E}{dV^2}$$

Normal Heusler  $\text{Co}_2\text{TiSn}$  and Heusler  $\text{Zr}_2\text{RhGa}$  compounds have space group Fm-3m (225), and inverse Heusler  $\text{Co}_2\text{TiSn}$  and Heusler  $\text{Zr}_2\text{RhGa}$  compounds have space group F-43m (216) [19]. We have calculated the structural properties for Full-Heusler  $\text{Co}_2\text{TiSn}$  and  $\text{Zr}_2\text{RhGa}$  compounds. The crystal structure of Full-Heusler  $\text{Co}_2\text{TiSn}$  and  $\text{Zr}_2\text{RhGa}$  compounds are shown in Figure 3. The total energy as function of the volume for normal and inverse Heusler  $\text{Co}_2\text{TiSn}$ ,  $\text{Zr}_2\text{RhGa}$  compounds are shown in Figure 4 (a-d). The optimized structural parameters are calculated from the equation of state (EOS) and tabulated in Table 1

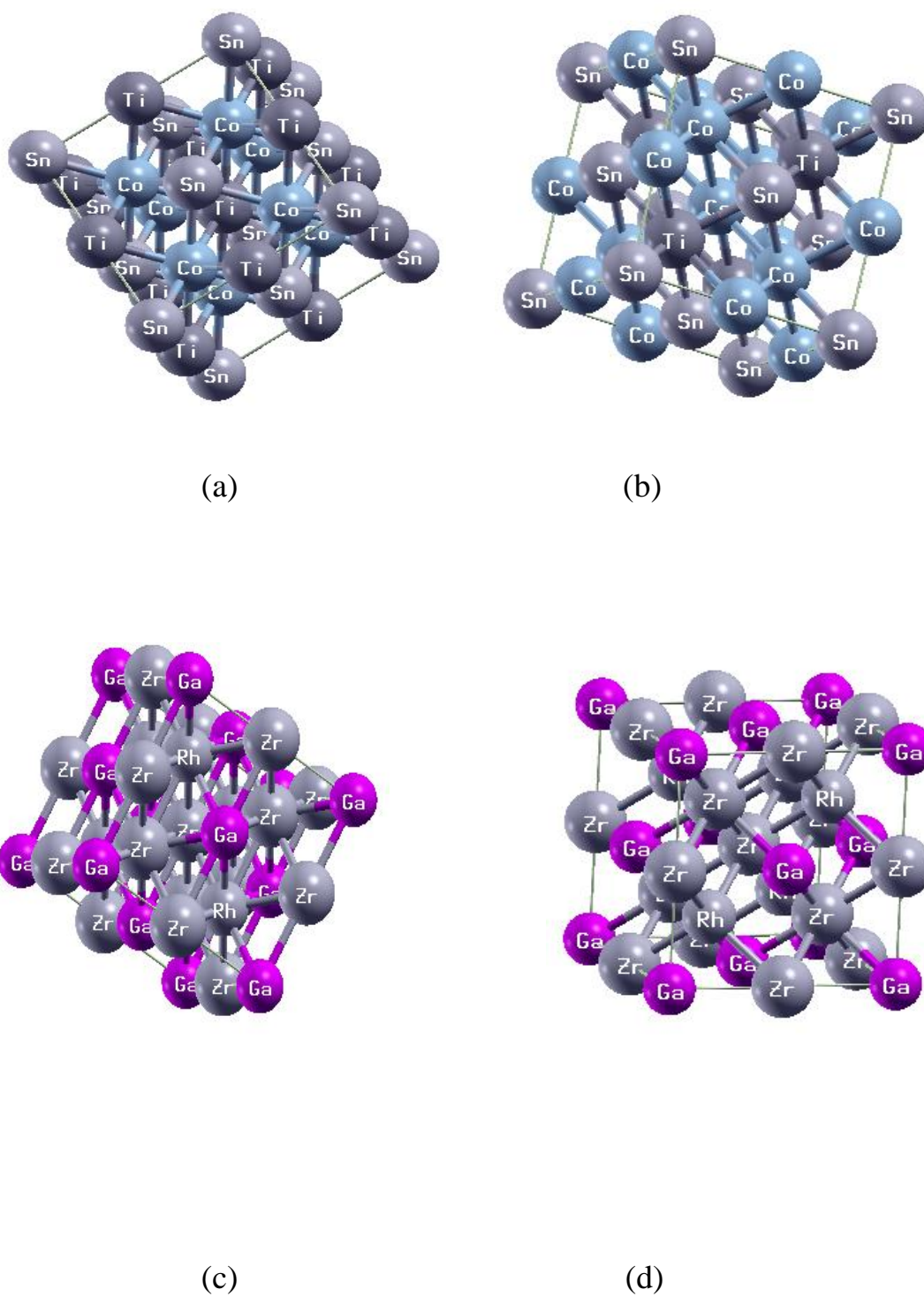
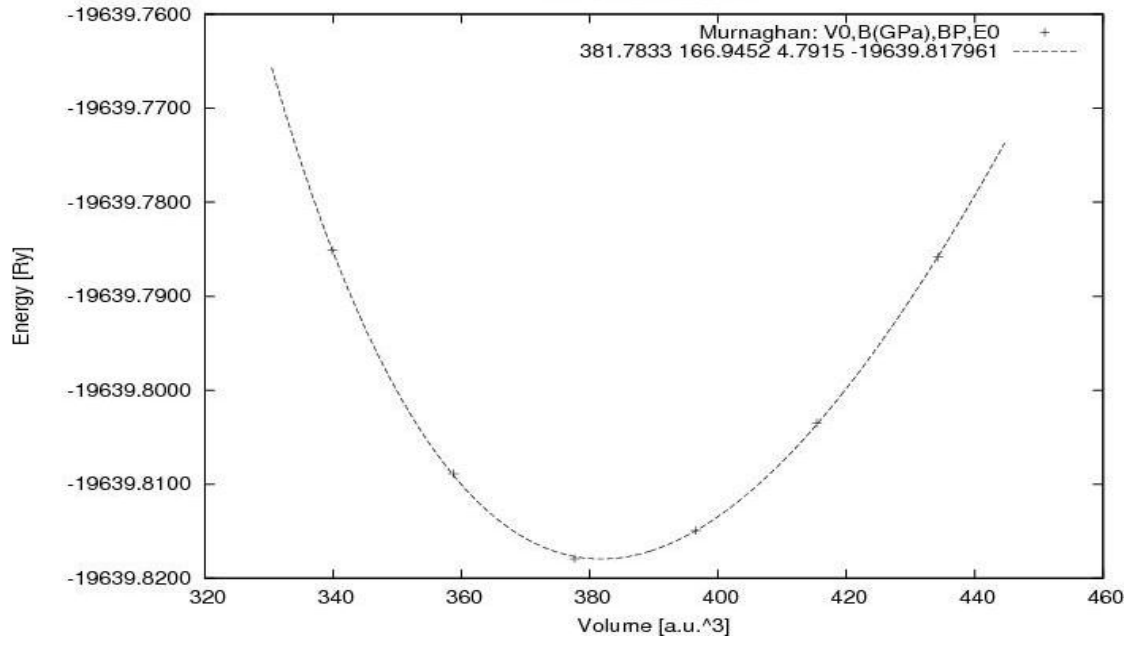
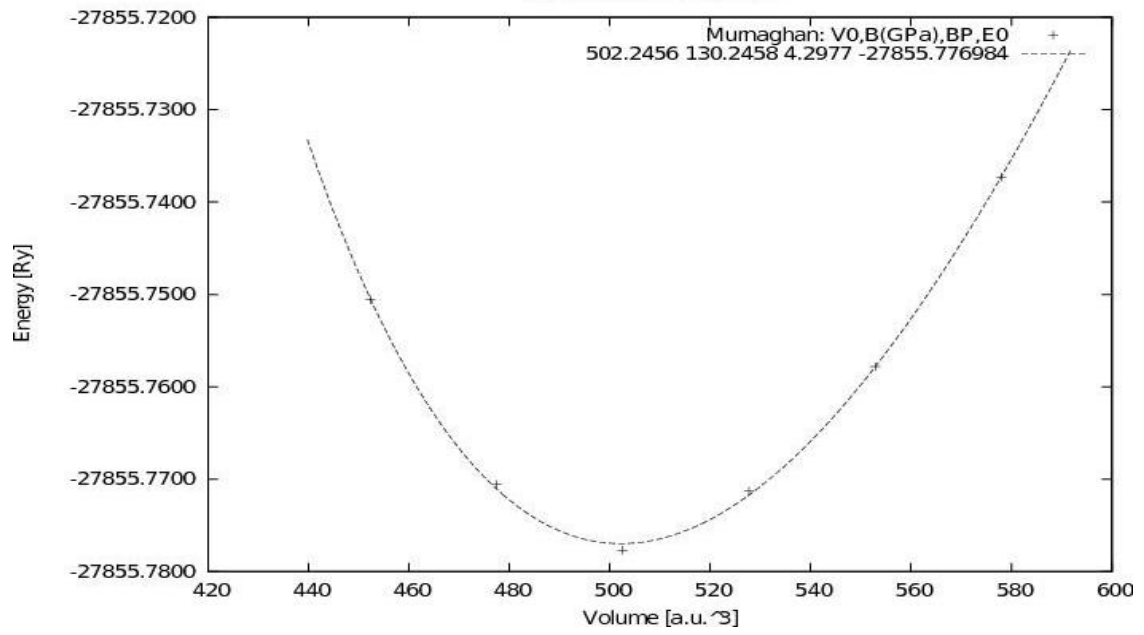


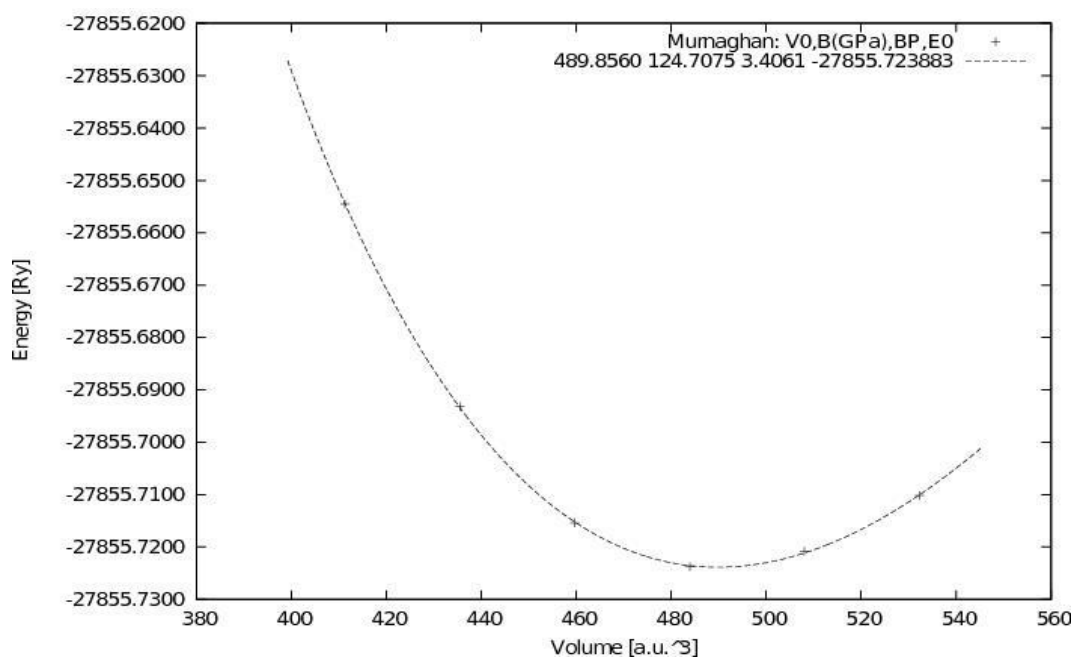
**Figure 3:** The crystal structure of (a) normal Heusler  $\text{Co}_2\text{TiSn}$  (b) inverse Heusler  $\text{Co}_2\text{TiSn}$  (c) normal Heusler  $\text{Zr}_2\text{RhGa}$  (d) inverse Heusler  $\text{Zr}_2\text{RhGa}$  compounds.



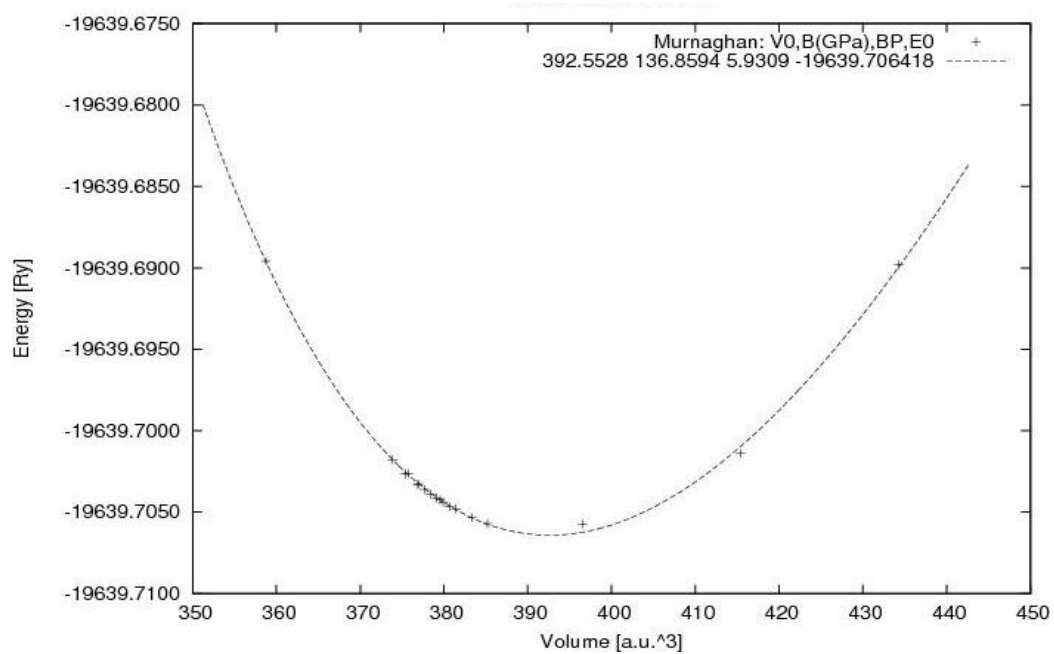
(a)



(b)



(c)



(d)

**Figure 4:** Total energy as function of the volume for (a) normal  $\text{Co}_2\text{TiSn}$  (b) normal Heusler  $\text{Zr}_2\text{RhGa}$  and (c) inverse  $\text{Zr}_2\text{RhGa}$  (d) inverse  $\text{Co}_2\text{TiSn}$  compounds.

The estimated lattice parameter (a), bulk modulus (B) and pressure derivative (B') at zero pressure are tabulated in Table 1 :

**Table 1: Calculated lattice parameter(a), bulk modulus(B), pressure derivative (B') for normal and inverse Heusler  $\text{Co}_2\text{TiSn}$  and  $\text{Zr}_2\text{RhGa}$  compounds.**

Compounds	Reference	Lattice parameter(a) Å	B (GPa)	B' (GPa)
Normal $\text{Co}_2\text{TiSn}$	Present	6.094	166.932	4.627
	Experimental	6.072 [19]	-	-
Normal $\text{Zr}_2\text{RhGa}$	Present	6.679	134.1	4.062
Inverse $\text{Co}_2\text{TiSn}$	Present	6.151	139.179	3.807
Inverse $\text{Zr}_2\text{RhGa}$	Present	6.619	129.319	5.073
	Theoretical	6.64 [26]	-	-

Table 1 shows that our calculated lattice parameter is in good agreement with the experimental lattice parameter for normal Heusler  $\text{Co}_2\text{TiSn}$  compound. The calculated lattice parameter of normal Heusler  $\text{Co}_2\text{TiSn}$  compound is slightly overestimated the experimental lattice parameter with 0.36% larger [19] .

Our calculated lattice parameter of inverse Heusler  $\text{Zr}_2\text{RhGa}$  compound is found to be closer to the other theoretical result [26].

### 3.3 Magnetic Properties

In this part, the total and partial magnetic moments for normal Heusler  $\text{Co}_2\text{TiSn}$  and Heusler  $\text{Zr}_2\text{RhGa}$ , and inverse Heusler  $\text{Co}_2\text{TiSn}$  and Heusler  $\text{Zr}_2\text{RhGa}$  Compounds were calculated, and compared with the experimental and other theoretical results as shown in Tables 2 and 3.

**Table 2: Total magnetic moment for normal and inverse Heusler  $\text{Co}_2\text{TiSn}$  Compounds.**

Compounds		Magnetic Moment ( $\mu_B$ )					Total magnetic moment ( $\mu_B$ )
		Co	Co	Ti	Sn	Interstitial	
Normal $\text{Co}_2\text{TiSn}$	Present	1.32398	1.32398	0.19866	0.00709	0.47779	1.9786
	Experimental Result	-	-	-	-	-	2 [19]
Inverse $\text{Co}_2\text{TiSn}$	Present	0.46092	1.54481	0.25961	0.01579	0.12165	1.64026

**Table 3: Total magnetic moment for normal and inverse Heusler  $\text{Zr}_2\text{RhGa}$  Compound.**

Compounds		Magnetic Moment ( $\mu_B$ )					Total magnetic moment ( $\mu_B$ )
		Zr	Zr	Rh	Ga	Interstitial	
Normal $\text{Zr}_2\text{RhGa}$	Present	0	0	0	0	0	0
Inverse $\text{Zr}_2\text{RhGa}$	Present	0.88019	0.44447	0.15415	0.00905	0.50214	1.99
	Theoretical Result	-	-	-	-	-	2 [26]

The integer value of the total magnetic moment ( $\mu_B$ ) is characteristic of half-metallic materials.

We noticed that the total magnetic moment are found to be in the range from 1.64026 to 2  $\mu_B$ . We found that the normal and inverse Heusler  $\text{Co}_2\text{TiSn}$  and inverse Heusler  $\text{Zr}_2\text{RhGa}$  compounds are ferromagnetic compounds. The total magnetic moment for normal  $\text{Zr}_2\text{RhGa}$  compound is 0  $\mu_B$  which means it does not have magnetic behavior.

Present results show that the calculated total magnetic moment of normal Heusler  $\text{Co}_2\text{TiSn}$  compound is underestimated the experimental value with 1.07% less[19]. Our calculated total magnetic moment of inverse Heusler  $\text{Zr}_2\text{RhGa}$  compound is found to be closer to the other theoretical result [26]. Present total magnetic moment results are to some extent compatible with experimental and theoretical results. The calculated total spin magnetic moments are clearly integral values and are in agreement with the Slater-Pauling rule [37].

### **3.4 Electronic Properties**

In this part, the band structure, the total and partial density of states for normal Heusler  $\text{Co}_2\text{TiSn}$  and Heusler  $\text{Zr}_2\text{RhGa}$ , and inverse Heusler  $\text{Co}_2\text{TiSn}$  and Heusler  $\text{Zr}_2\text{RhGa}$  compounds were calculated.

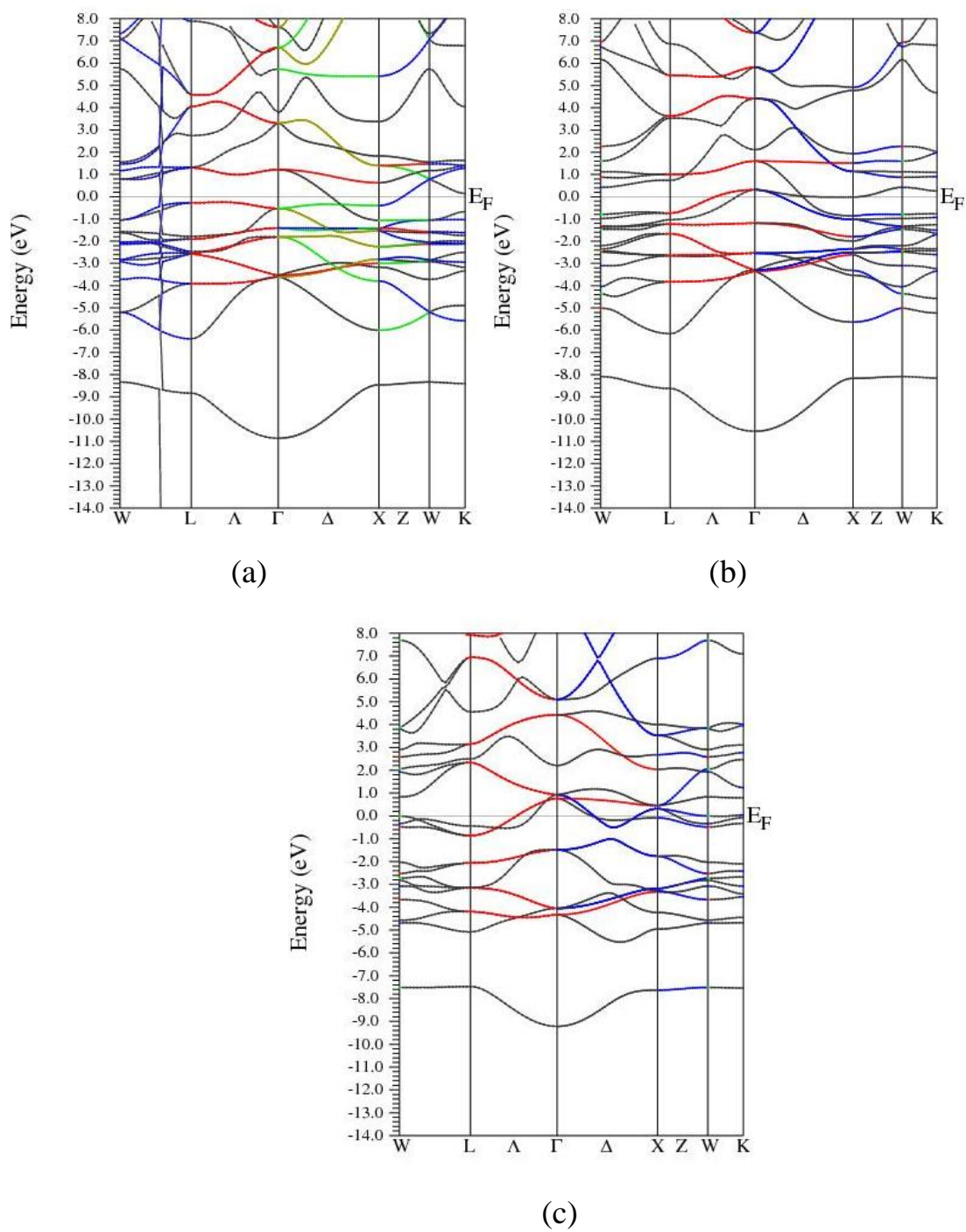
It is clear from the band structure and density of states that the normal Heusler  $\text{Co}_2\text{TiSn}$  and inverse Heusler  $\text{Zr}_2\text{RhGa}$  compounds both have a half-metallic behavior, which means at spin up the materials behave as metallic nature while at spin down the materials behave as semiconducting nature, and inverse Heusler  $\text{Co}_2\text{TiSn}$  and normal Heusler  $\text{Zr}_2\text{RhGa}$  compounds both have a metallic behavior.

Figure 5 (a, b and c) shows that the band structure spin up of normal and inverse Heusler  $\text{Co}_2\text{TiSn}$  and inverse Heusler  $\text{Zr}_2\text{RhGa}$  compounds have metallic nature by using PBE-GGA method. Figure 6(a and c) shows that the band structure spin down of normal Heusler  $\text{Co}_2\text{TiSn}$  and inverse Heusler  $\text{Zr}_2\text{RhGa}$  compounds have an indirect energy band gap using PBE-GGA method. The values of the energy band gaps of spin down are calculated for normal Heusler  $\text{Co}_2\text{TiSn}$  and inverse Heusler  $\text{Zr}_2\text{RhGa}$  compounds using PBE-GGA method. The energy band gaps of normal Heusler  $\text{Co}_2\text{TiSn}$  and inverse Heusler  $\text{Zr}_2\text{RhGa}$  compounds are found to be 0.482 eV and 0.573 eV, respectively as shown in Tables 4 and 5.

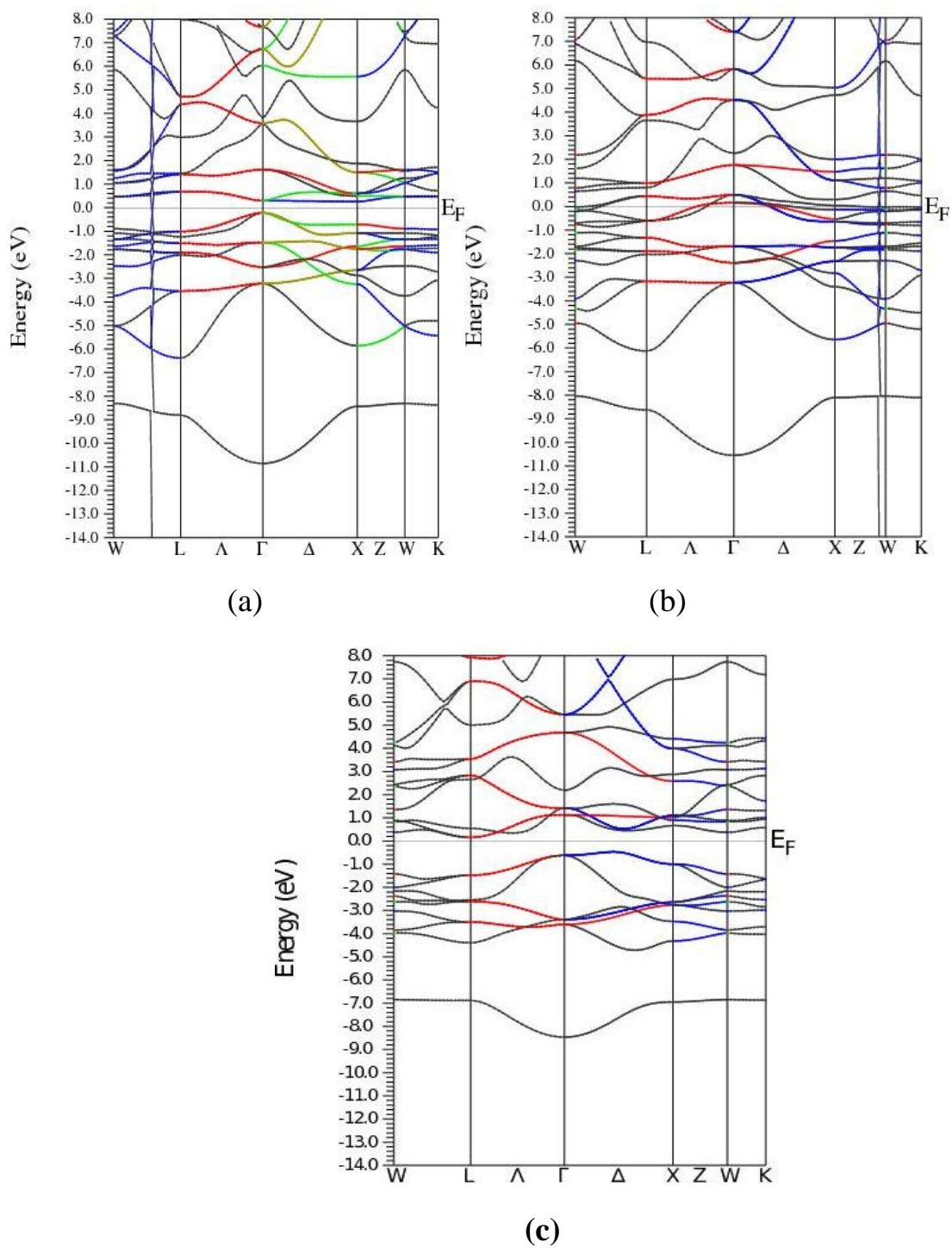
Figure 6b shows that the spin up of inverse Heusler  $\text{Co}_2\text{TiSn}$  has metallic behavior using PBE-GGA method. The band structure of normal Heusler  $\text{Co}_2\text{TiSn}$  and inverse Heusler  $\text{Zr}_2\text{RhGa}$  are also calculated by using mBJ-GGA.

Figure 7 shows that the normal Heusler  $\text{Zr}_2\text{RhGa}$  compound has metallic behavior. Figure 8 (a and b) also shows that the spin up of normal Heusler  $\text{Co}_2\text{TiSn}$  and inverse Heusler  $\text{Zr}_2\text{RhGa}$  compounds both have metallic behavior using mBJ-GGA method.

Figure 9 (a and b) shows the energy band gap within mBJ-GGA method for normal Heusler  $\text{Co}_2\text{TiSn}$  and inverse Heusler  $\text{Zr}_2\text{RhGa}$  compounds is still indirect band gap and the energy gap increases for normal  $\text{Co}_2\text{TiSn}$  to 1.430 eV and for inverse  $\text{Zr}_2\text{RhGa}$  to 0.641 eV at spin down.



**Figure 5:** Band structure spin up by using PBE-GGA method for (a) normal  $\text{Co}_2\text{TiSn}$  (b) inverse  $\text{Co}_2\text{TiSn}$  (c) inverse  $\text{Zr}_2\text{RhGa}$  compounds



**Figure 6:** Band structure spin down by using PBE-GGA method for (a) normal  $\text{Co}_2\text{TiSn}$  (b) inverse  $\text{Co}_2\text{TiSn}$  (c) inverse  $\text{Zr}_2\text{RhGa}$  compounds

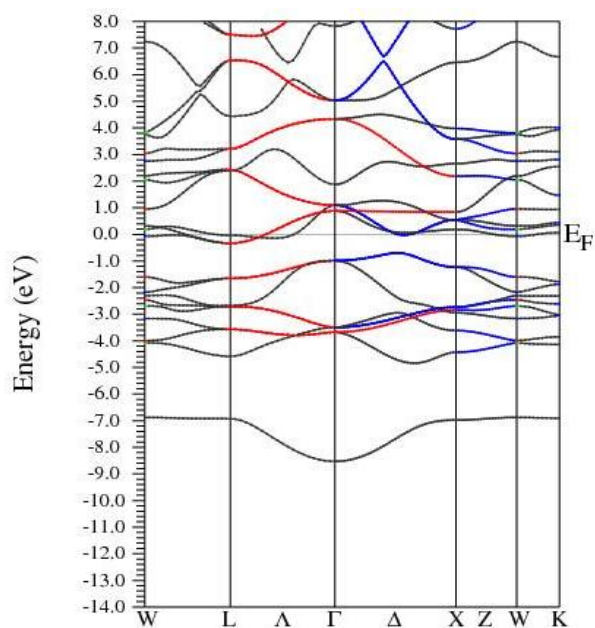


**Figure 7:** Band structure by using PBE-GGA method for normal  $Zr_2RhGa$  compound .

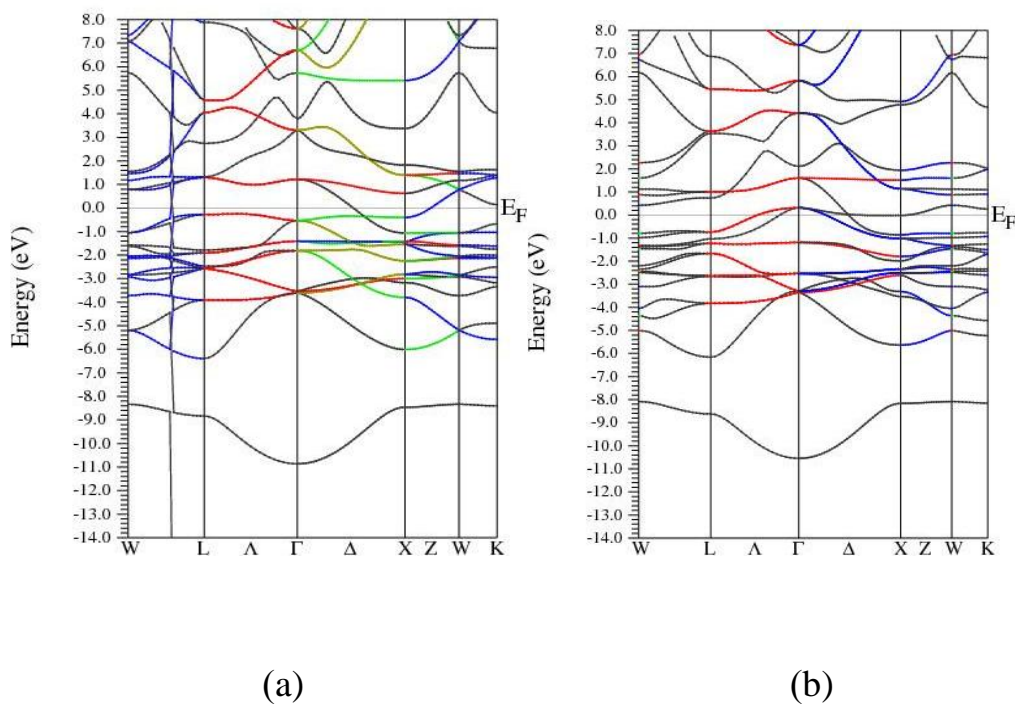


**Figure 8:** Band structure spin up by using mBJ-GGA method for (a) normal  $Co_2TiSn$   
(b) inverse  $Zr_2RhGa$  compounds

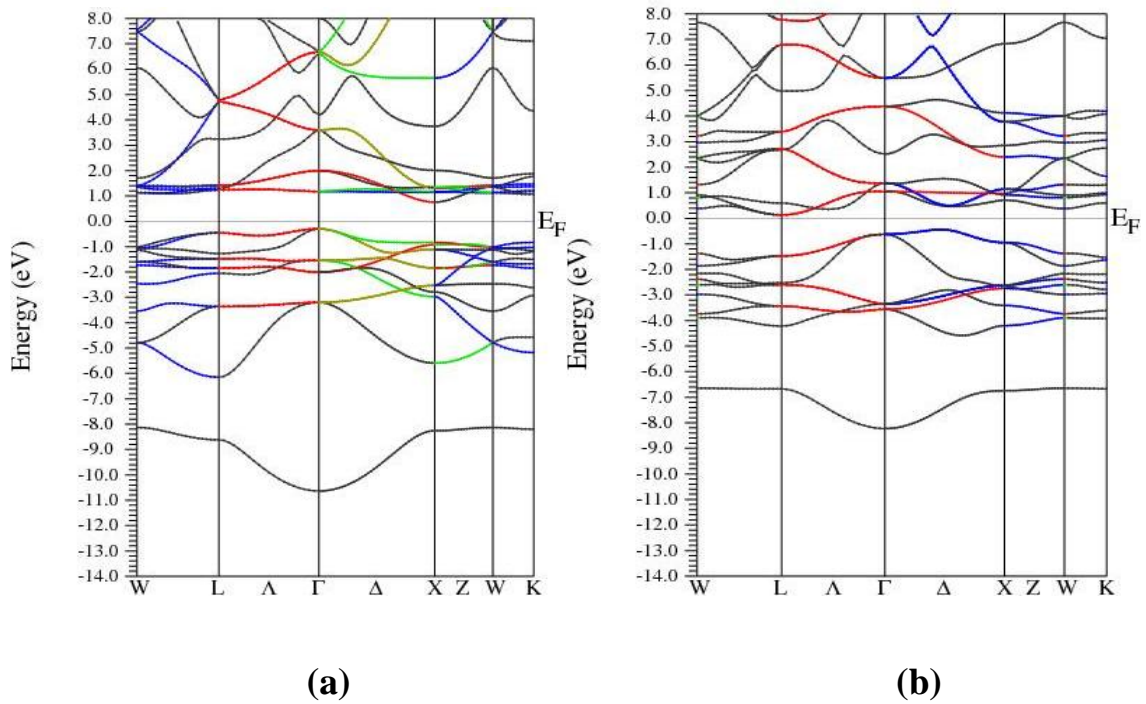


**Figure 9:** Band structure spin down by using mBJ-GGA method for (a) normal  $\text{Co}_2\text{TiSn}$  (b) inverse  $\text{Zr}_2\text{RhGa}$  compounds .

The band gap types and high symmetry lines are presented in Tables 4 and 5:

**Table 4: Energy band gaps for normal Heusler  $\text{Co}_2\text{TiSn}$  and normal Heusler  $\text{Zr}_2\text{RhGa}$  Compounds using PBE-GGA and mBJ-GGA methods Compounds.**

Compounds	Band gap type	High Symmetry Lines	Eg-PBE-GGA (eV)	Eg-mBJ-GGA (eV)
$\text{Co}_2\text{TiSn}$	Indirect	$\Gamma$ -X	0.482	1.430
$\text{Zr}_2\text{RhGa}$	Metallic	-	-	-

**Table 5: Energy band gaps for inverse Heusler  $\text{Co}_2\text{TiSn}$  and inverse Heusler  $\text{Zr}_2\text{RhGa}$  Compounds using PBE-GGA and mBJ-GGA methods.**

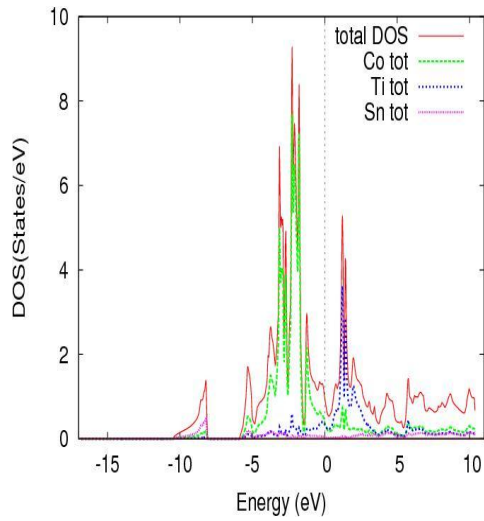
Compounds	Band gap type	High Symmetry Lines	Eg-PBE-GGA (eV)	Eg-mBJ-GGA (eV)
$\text{Co}_2\text{TiSn}$	Metallic	-	-	-
$\text{Zr}_2\text{RhGa}$	Indirect	L- $\Delta$	0.573	0.641

Total and partial density of states of spin up and spin down for normal Heusler  $\text{Co}_2\text{TiSn}$  and inverse Heusler  $\text{Zr}_2\text{RhGa}$  compounds are shown in Figures (10 – 16). Density of state figures (10-16) show also half metallic property for normal  $\text{Co}_2\text{TiSn}$  and inverse  $\text{Zr}_2\text{RhGa}$  compounds with existing small energy band gap in the spin down direction, and this means that these compounds have half metallic property. In the spin up of normal  $\text{Co}_2\text{TiSn}$  (Figure 10), the valence band is due to d-state of Co, s-state and p-state of Sn and small contribution from Ti d-state, while the conduction band is due to d-state of Ti and small contribution from Sn p-state. In spin down of normal  $\text{Co}_2\text{TiSn}$  (Figure 11), the valence band is due to Co d-state, Ti d-state and Sn s-state and p-state, while the conduction band is due to Co d-state and Ti d-state and small contribution from s-state and p-state.

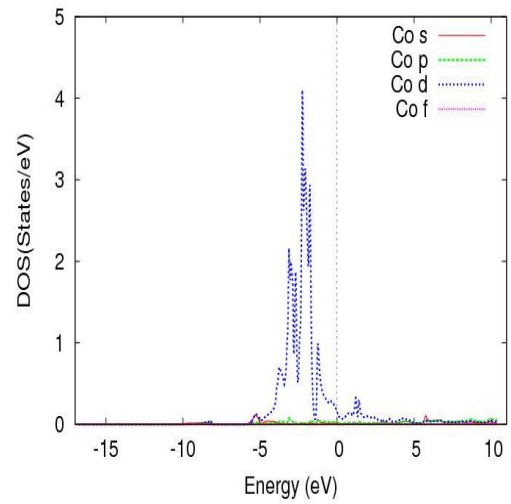
In normal  $\text{Zr}_2\text{RhGa}$  (Figure 12), the valence band is due to Rh d-state and Ga s-state, and small contribution from Zr near to fermi level due to Zr d-state, and the conduction band is due to Zr d-state, and small contribution of Rh due to d-state.

In spin up of inverse  $\text{Co}_2\text{TiSn}$  (Figure 13), the valence band is due to Co d-state, Sn s-state and p-state, and small contribution from Ti d-state, and the conduction band is due to Ti d-state and small contribution from s-state and p-state. In spin down of inverse  $\text{Co}_2\text{TiSn}$ (Figure 14), the valence band is due to Co d-state near to fermi level and Sn s-state and p-state, and small contribution from Ti d-state, and the conduction band is due to Co d-state near to fermi energy and Ti d-state, and small contribution from Sn s-state and p-state.

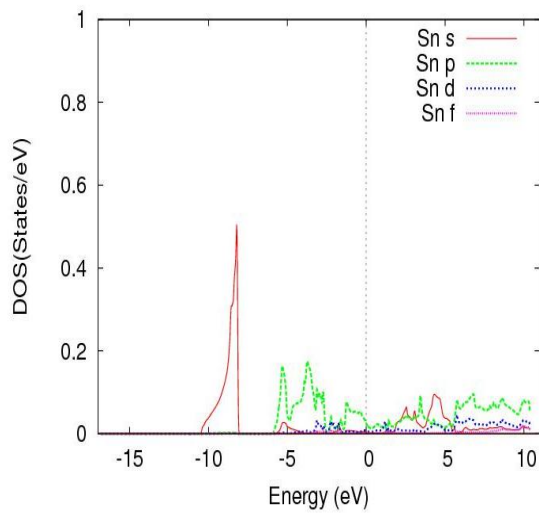
In spin up of inverse  $\text{Zr}_2\text{RhGa}$  (Figure 15), the valence band is due to Rh d-state, Ga d-state, and small contribution from Zr d-state near to fermi energy level, and the conduction band is due to Zr d-state near to fermi energy level. In spin down of inverse  $\text{Zr}_2\text{RhGa}$  (Figure 16), the valence band is due to Rh d-state , Ga d-state and small contribution from Zr d-state, and the conduction band is due to Zr d-state near to fermi energy level, and small contribution from Rh and Ga d-states .



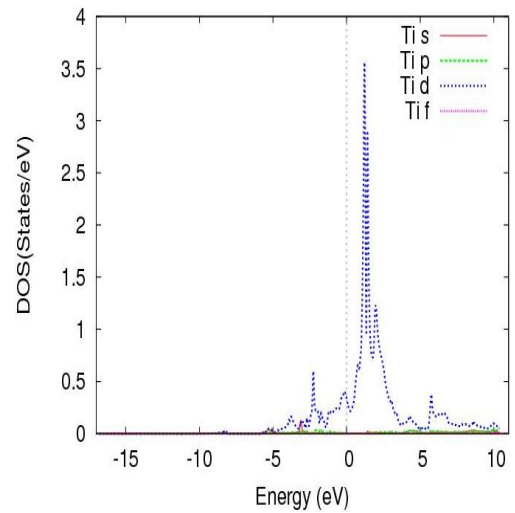
(a)



(b)



(c)



(d)

**Figure 10 :** (a) Total density of states of spin up for normal  $\text{Co}_2\text{TiSn}$  and partial density of states of spin up for (b) Co atom (c) Ti atom (d) Sn atom of normal  $\text{Co}_2\text{TiSn}$  compound.

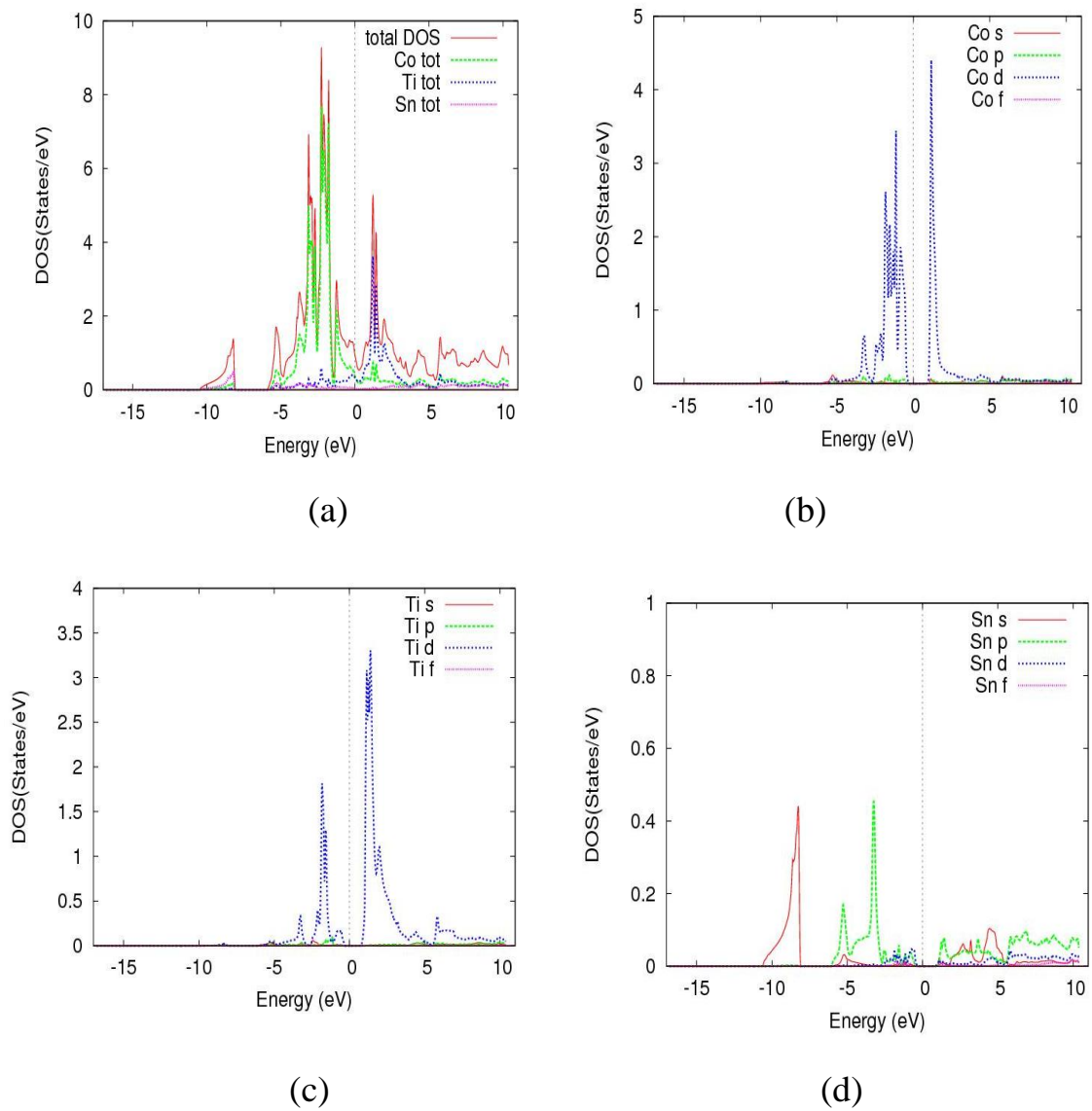


**Figure 11:** (a) Total density of states of spin down for normal  $\text{Co}_2\text{TiSn}$  compound and partial density of states of spin down for (b) Co atom (c) Ti atom (d) Sn atom of normal  $\text{Co}_2\text{TiSn}$  compound .

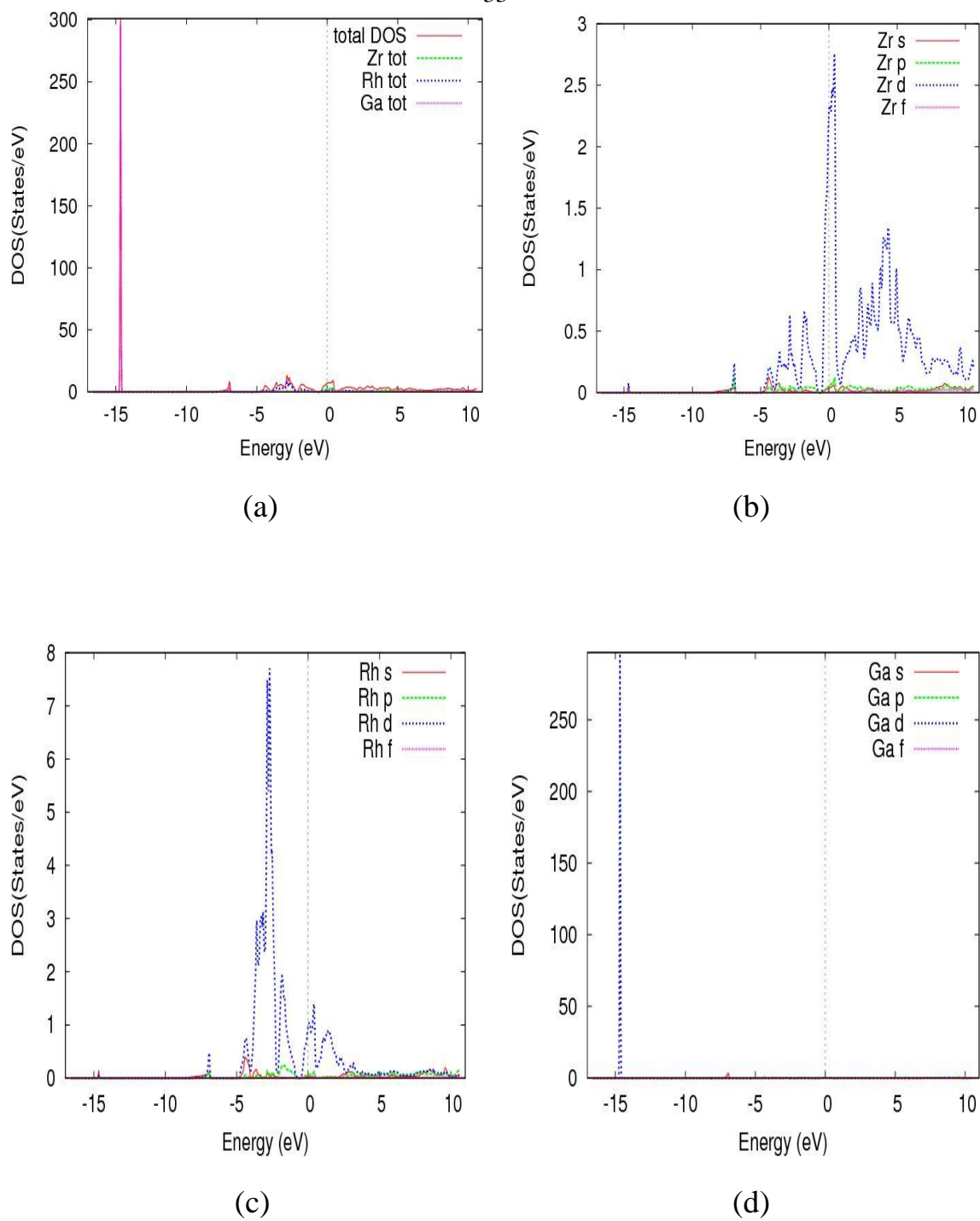


**Figure 12:** (a) Total density of states for normal  $Zr_2RhGa$  and partial density of states for (b) Zr atom (c) Rh atom (d) Ga atom of normal  $Zr_2RhGa$  compound.

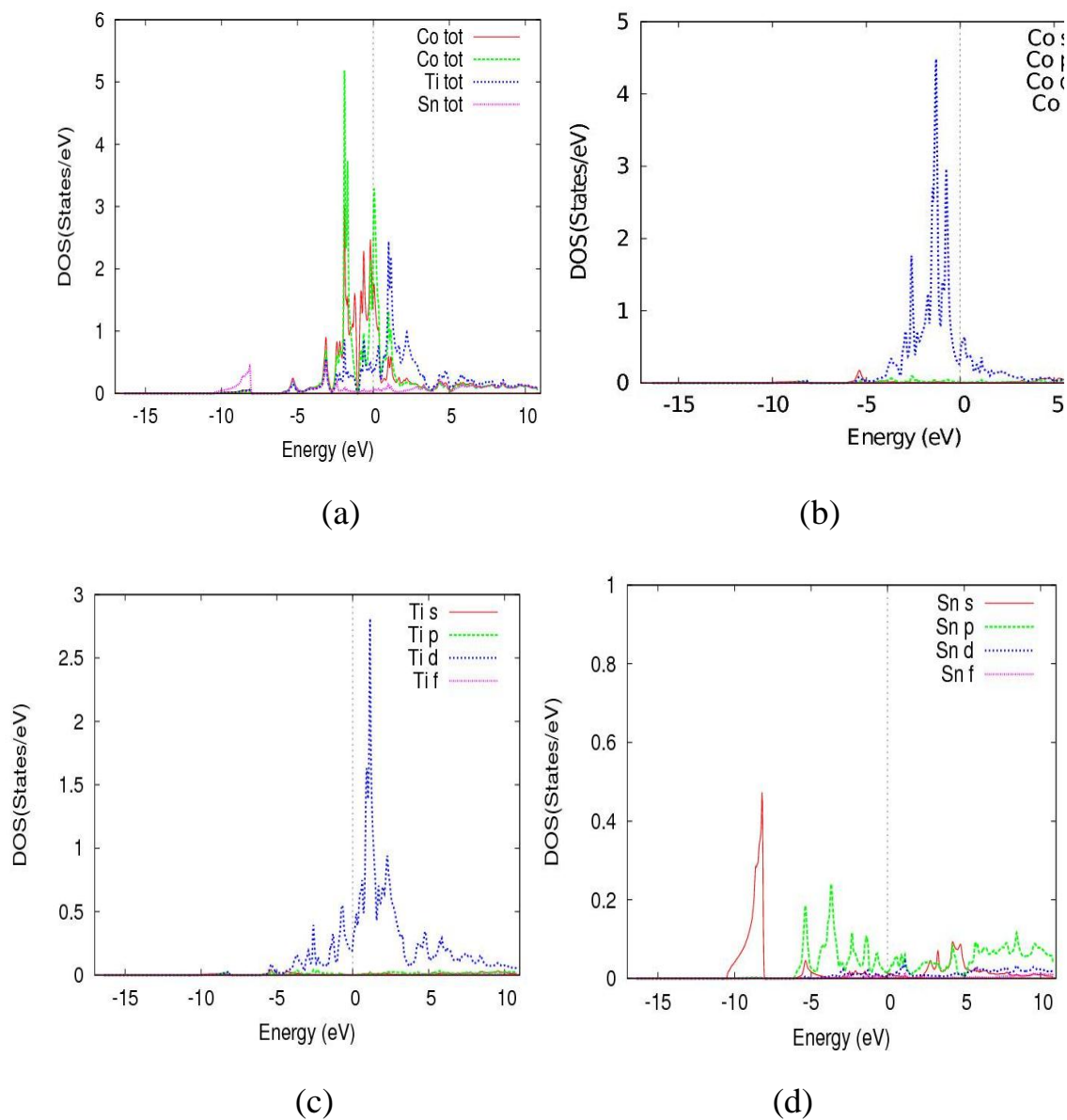


**Figure 13:** (a) Total density of states of spin up for inverse  $\text{Co}_2\text{TiSn}$  and partial density of states of spin up for (b) Co atom (c) Ti atom (d) Sn atom of inverse  $\text{Co}_2\text{TiSn}$  compound.

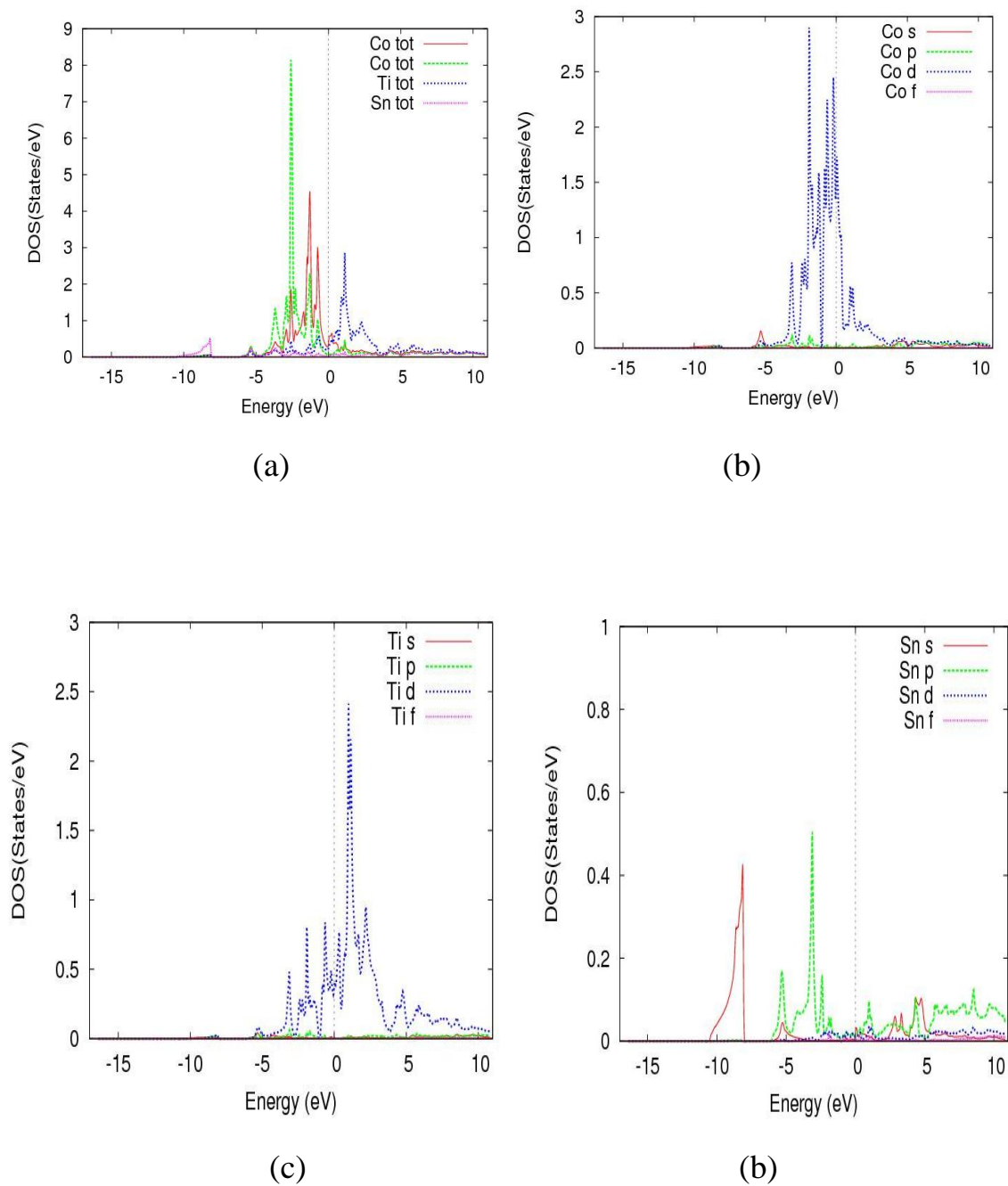


**Figure 14:** (a) Total density of states of spin down for inverse  $\text{Co}_2\text{TiSn}$  and partial density of states of spin down for (b) Co atom (c) Ti atom (d) Sn atom of inverse  $\text{Co}_2\text{TiSn}$  compound.

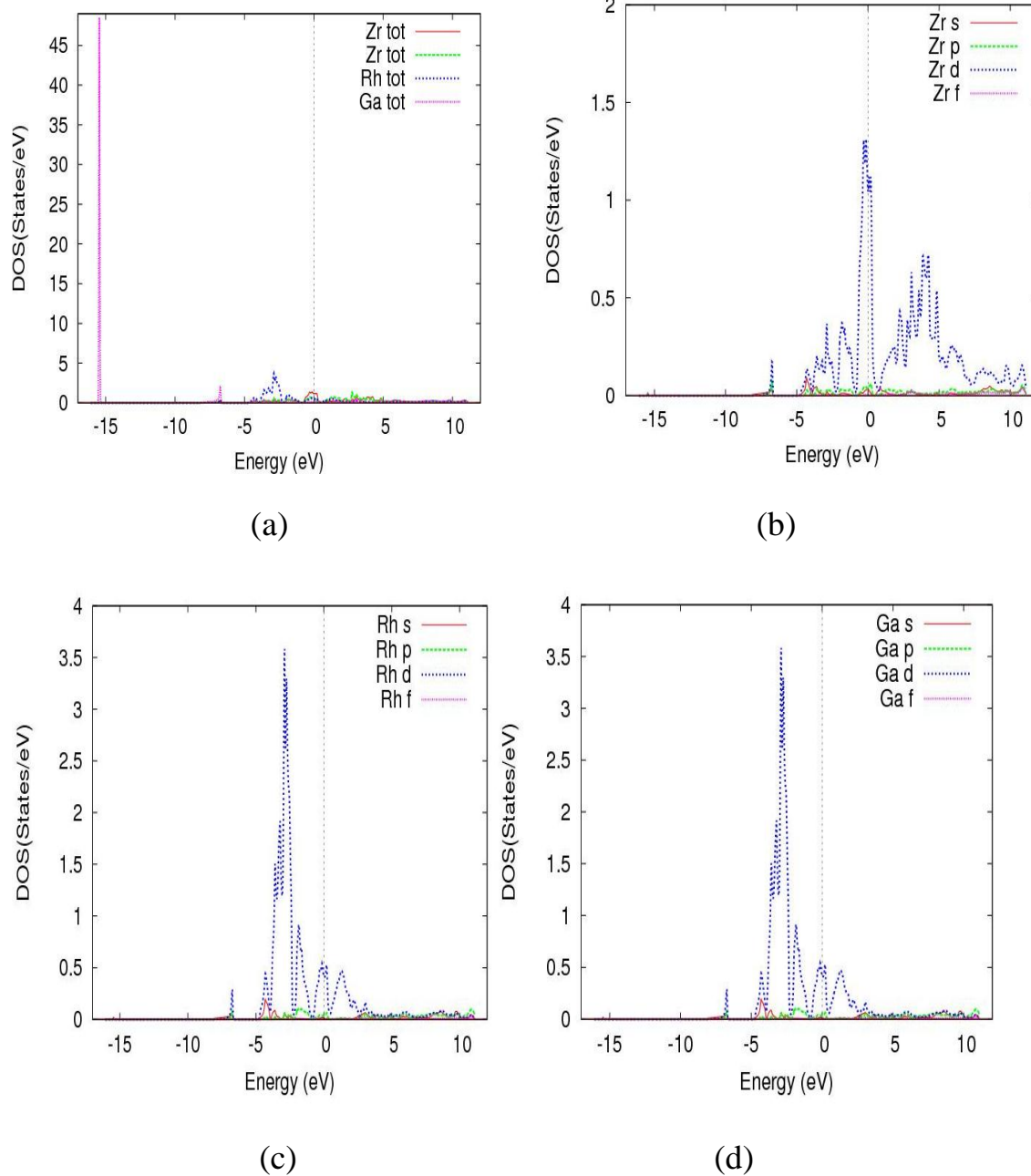


**Figure 15:** (a) Total density of states of spin up for inverse  $Zr_2RhGa$  and partial density of states of spin up for (b) Zr atom (c) Rh atom (d) Ga atom of inverse  $Zr_2RhGa$  compound.

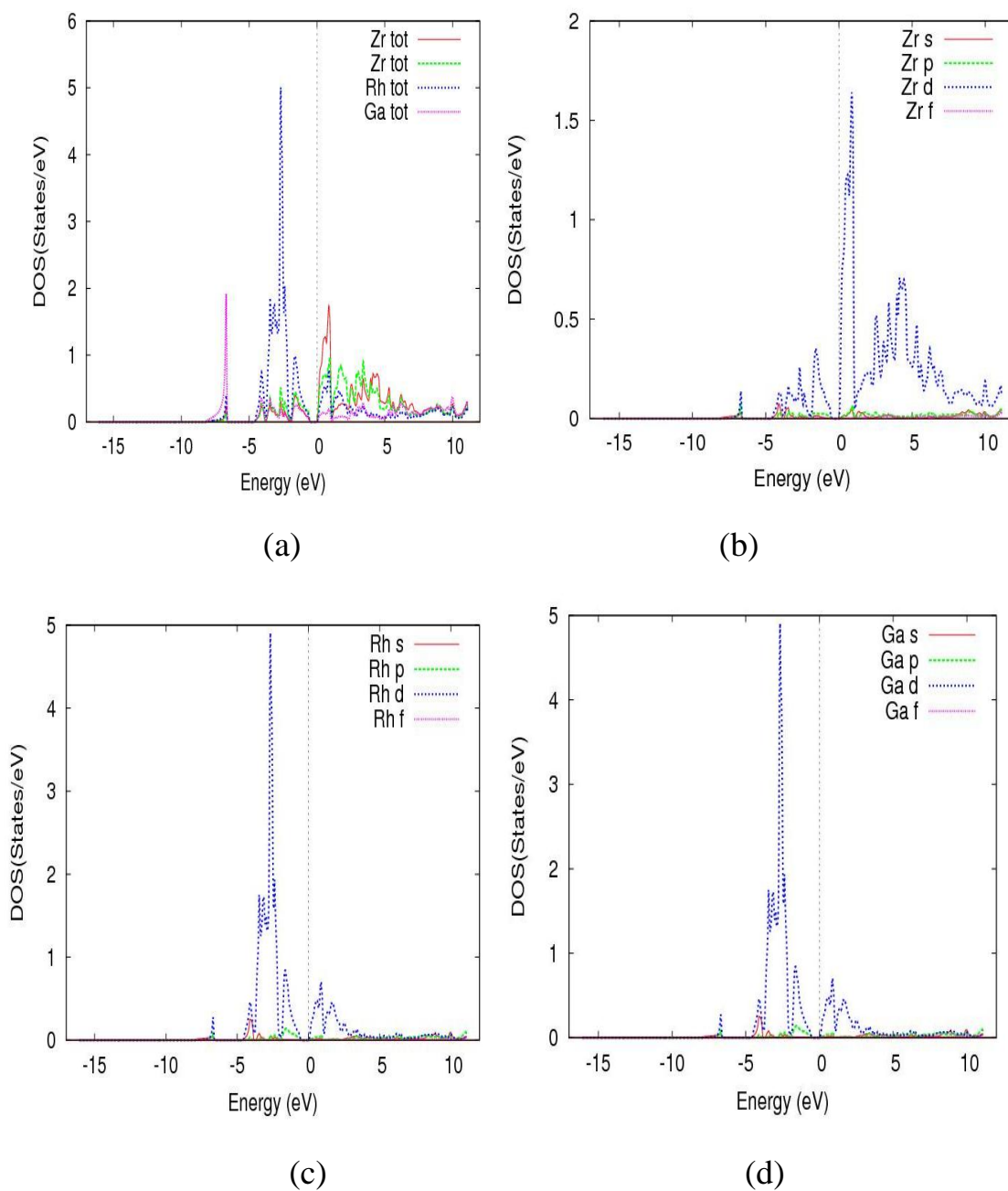


**Figure 16:** (a) Total density of states of spin down for inverse  $Zr_2RhGa$  and partial density of states of spin down for (b) Zr atom (c) Rh atom (d) Ga atom of inverse  $Zr_2RhGa$  compound.

### 3.5 Elastic Properties

In this part, elastic constants ( $C_{ii}$ ), bulk modulus (B), shear modulus (S), B/S ratio, Young's modulus (Y), Poisson's ratio ( $\nu$ ) and anisotropic factor (A) of the normal  $\text{Co}_2\text{TiSn}$  and inverse  $\text{Zr}_2\text{RhGa}$  compounds were calculated. For a cubic crystal, the standard mechanical stability is  $C_{11} > 0$ ,  $C_{11} - C_{12} > 0$ ,  $C_{11} + 2C_{12} > 0$  and  $C_{44} > 0$  [38].

Present calculations satisfied all the above conditions. We noticed that the normal Heusler  $\text{Co}_2\text{TiSn}$  and inverse Heusler  $\text{Zr}_2\text{RhGa}$  compounds are found to be mechanically stable, while inverse Heusler  $\text{Co}_2\text{TiSn}$  and normal Heusler  $\text{Zr}_2\text{RhGa}$  compounds are mechanically unstable. In our calculation, we focused on normal Heusler  $\text{Co}_2\text{TiSn}$  and inverse Heusler  $\text{Zr}_2\text{RhGa}$  Compounds. For the face center cubic crystal, the bulk modulus and shear modulus were calculated using Voigt and Reuss approximations, Bulk modulus for cubic structure can be calculated from the following equations [39,40]:

$$B = \frac{1}{3}(C_{11} + 2C_{12}) \quad (23)$$

Voigt Shear modulus  $S_V$  and Reuss shear modulus  $S_R$  are given by the following two equations:

$$S_V = \frac{1}{5}(C_{11} - C_{12} + 3C_{44}) \quad (24)$$

$$S_R = \frac{5c_{44}(c_{11}-c_{12})}{4c_{44}+3(c_{11}-c_{12})} \quad (25)$$

The average value of Voigt shear modulus and Reuses shear modulus is called Hill shear modulus ,and can be estimated from the following equation [39,40] :

$$S_H = \frac{1}{2}(S_v + S_R) \quad (26)$$

Young's modulus (Y) is defined as the ratio of the stress to strain, and given by:

$$Y = \frac{9S_H B}{(S_H + 3B)} \quad (27)$$

Poisson's ratio and anisotropic factor can be computed by using bulk and shear moduli, Poisson's ratio and anisotropic factor can be given by:

$$V = \frac{3B - 2S}{2(3B + S)} \quad (28)$$

$$A = \frac{2c_{44}}{c_{11} - c_{12}} \quad (29)$$

Elastic constants, Voight bulk modulus (B), Voight shear modulus (S), B/S ratio, Voight Young's modulus (Y), Voight Poisson's ratio (v) and anisotropic factor (A) are presented in Table 6:

**Table 6: Elastic constants for normal Co<sub>2</sub>TiSn and inverse Zr<sub>2</sub>RhGa Full Heusler Compounds.**

<b>Materials</b>	<b>C<sub>11</sub> (GPa)</b>	<b>C<sub>12</sub> (GPa)</b>	<b>C<sub>44</sub> (GPa)</b>	<b>B (GPa)</b>	<b>S (GPa)</b>	<b>B/S</b>	<b>Y (GPa)</b>	<b>V</b>	<b>A</b>
Normal Co <sub>2</sub> TiSn	246.976	136.962	109.226	173.633	87.53	0.841	224.83	0.284	1.985
Normal Zr <sub>2</sub> RhGa	118.2706	141.5202	2.1653	133.77	-3.350	-39.931	-10.13	0.512	-0.186
Inverse Co <sub>2</sub> TiSn	120.027	151.389	104.594	140.934	56.482	2.495	149.48	0.323	-6.67
Inverse Zr <sub>2</sub> RhGa	145.279	116.5186	70.4579	126.105	48.026	2.6257	127.85	0.331	4.9

The Bulk (B) or shear modulus (S) measures the hardness of materials [37]. The ratio B/S measures the ductility and brittleness of the materials. When  $B/S > 1.75$ , the materials behave in a ductile nature, otherwise it behaves in a brittle nature [38]. In the present calculations, the B/S ratio of normal Heusler  $\text{Co}_2\text{TiSn}$ , normal Heusler  $\text{Zr}_2\text{RhGa}$ , inverse Heusler  $\text{Co}_2\text{TiSn}$ , and inverse Heusler  $\text{Zr}_2\text{RhGa}$  compounds are 0.841, -39.931, 2.495 and 2.6257, respectively, The normal Heusler  $\text{Co}_2\text{TiSn}$  and normal Heusler  $\text{Zr}_2\text{RhGa}$  both have brittle nature, while inverse Heusler  $\text{Co}_2\text{TiSn}$  and inverse Heusler  $\text{Zr}_2\text{RhGa}$  both have ductile nature.

Young modulus (Y) measures the stiffness of materials. The highest the value of Young modulus (Y), the stiffest is the material and the solids will have covalent bonds. The Poisson ratio ( $\nu$ ) measures the stability of the material and provides useful information about the nature of the bonding [39]. When Poisson ratio ( $\nu$ ) is greater than  $1/3$ , the materials behave in a ductile nature. Otherwise, it behaves in a brittle nature [40], and if the value of Poisson's ratio is greater than 0.25, the material will have ionic bond; otherwise, the material has covalent bond.

In the present calculations, the  $\nu$  of normal Heusler  $\text{Co}_2\text{TiSn}$ , normal Heusler  $\text{Zr}_2\text{RhGa}$ , inverse Heusler  $\text{Co}_2\text{TiSn}$ , and inverse Heusler  $\text{Zr}_2\text{RhGa}$  compounds are found to be 0.284, 0.512, 0.323, and 0.331, respectively, The normal Heusler  $\text{Co}_2\text{TiSn}$ , normal Heusler  $\text{Zr}_2\text{RhGa}$ , inverse Heusler  $\text{Co}_2\text{TiSn}$ , inverse Heusler  $\text{Zr}_2\text{RhGa}$  compounds have ionic bonds. Likewise, the elastic anisotropy is an important parameter to measure the degree of anisotropy of materials [41]. For an isotropic material, the value of A is

unity. Otherwise, the material has an elastic anisotropy [42]. In the present calculations, the  $A$  of normal Heusler  $\text{Co}_2\text{TiSn}$ , normal Heusler  $\text{Zr}_2\text{RhGa}$ , inverse Heusler  $\text{Co}_2\text{TiSn}$ , and inverse Heusler  $\text{Zr}_2\text{RhGa}$  compounds are found to be 1.985, -0.186, -6.67, 4.899, respectively and the normal Heusler  $\text{Co}_2\text{TiSn}$ , normal Heusler  $\text{Zr}_2\text{RhGa}$ , inverse Heusler  $\text{Co}_2\text{TiSn}$ , and inverse Heusler  $\text{Zr}_2\text{RhGa}$  Compounds are elastic anisotropy [43].

## Chapter Four

### Conclusion

In this work, the structural, electronic, magnetic and elastic properties for normal Heusler  $\text{Co}_2\text{TiSn}$  and inverse Heusler  $\text{Zr}_2\text{RhGa}$  Full Heusler compounds have been studied.

We found that normal Heusler  $\text{Co}_2\text{TiSn}$  compound and the inverse Heusler  $\text{Zr}_2\text{RhGa}$  compound have half-metallic behavior. The normal Heusler  $\text{Co}_2\text{TiSn}$  and inverse Heusler  $\text{Zr}_2\text{RhGa}$  compounds have an indirect energy gap of 0.482 eV and 0.573 eV using PBE-GGA method. It was shown that the energy band gap within mBJ-GGA for normal Heusler  $\text{Co}_2\text{TiSn}$  compound and for inverse Heusler  $\text{Zr}_2\text{RhGa}$  compound are still indirect band gap and the energy gap increases for normal Heusler  $\text{Co}_2\text{TiSn}$  to be 1.430 eV and for inverse Heusler  $\text{Zr}_2\text{RhGa}$  to be 0.641 eV.

The calculated total magnetic moment for these compounds are in the range from 1.64 to 2  $\mu_B$ , which means that present results are to some extent compatible with the experimental and theoretical results .

The elastic properties indicate that the normal Heusler  $\text{Co}_2\text{TiSn}$  compound and the inverse Heusler  $\text{Zr}_2\text{RhGa}$  compound are mechanically stable. B/S results show that the normal Heusler  $\text{Co}_2\text{TiSn}$  and normal Heusler  $\text{Zr}_2\text{RhGa}$  compounds both have brittle nature, while inverse Heusler  $\text{Co}_2\text{TiSn}$  and inverse Heusler  $\text{Zr}_2\text{RhGa}$  compounds both have ductile nature. The Poisson's ratio ( $\nu$ ) of normal Heusler  $\text{Co}_2\text{TiSn}$ , normal Heusler  $\text{Zr}_2\text{RhGa}$ , inverse Heusler  $\text{Co}_2\text{TiSn}$ , and inverse Heusler  $\text{Zr}_2\text{RhGa}$  compounds are

found to be 0.284, 0.512, 0.323, and 0.331, respectively. The normal Heusler  $\text{Co}_2\text{TiSn}$ , normal Heusler  $\text{Zr}_2\text{RhGa}$ , inverse Heusler  $\text{Co}_2\text{TiSn}$ , and inverse Heusler  $\text{Zr}_2\text{RhGa}$  compounds have ionic bonds. The  $A$  of normal Heusler  $\text{Co}_2\text{TiSn}$ , normal Heusler  $\text{Zr}_2\text{RhGa}$ , inverse Heusler  $\text{Co}_2\text{TiSn}$ , and inverse Heusler  $\text{Zr}_2\text{RhGa}$  compounds are found to be 1.985, -0.186, -6.67, 4.899, respectively, and the normal Heusler  $\text{Co}_2\text{TiSn}$  and normal Heusler  $\text{Zr}_2\text{RhGa}$ , inverse Heusler  $\text{Co}_2\text{TiSn}$ , and inverse Heusler  $\text{Zr}_2\text{RhGa}$  compounds are elastic anisotropy.

## References

1. R.A. de Groot, F.M. Mueller, P.G. van Engen, K.H.J. Buschow, **Phys. Rev. Lett.** 50 2024 (1983).
2. G. A. Prinz, **Science** 282 1660 (1998).
3. G.D. Liu, X.F. Dai, S.Y. Yu, Z.Y. Zhu, J.L. Chen, G.H. Wu, H. Zhu, and J.Q. Xiao, *Phys. Rev. B* 74 054435 (2006).
4. X.F. Dai, G.D. Liu, L.J. Chen, J.L. Chen, and G.H. Wu, **Solid State Commun.** 140 533 (2006).
5. G.D. Liu, X.F. Dai, H.Y. Liu, J.L. Chen, Y.X. Li, **Phys. Rev. B** 77 014424 (2008).
6. E. Bayar, N. Kervan, S. Kervan, *J. Magn. Mater.* 323 2945 (2011).
7. Q.L. Fang, J.M. Zhang, K.W. Xu, V. Ji, *J. Magn. Mater.* 345 171 (2013).
8. N. Kervan, S. Kervan, *J. Magn. Mater.* 324 645 (2012).
9. H.Y. Jia, X.F. Dai, L.Y. Wang, R. Liu, X.T. Wang, P.P. Li, Y.T. Cui, G.D.Liu, *J. Magn. Mater.* 367 33(2014).
10. A. Birsan, P. Palade, V. Kuncser, *J. Magn. Mater.* 331 109 (2013).

11. Yamamoto M, Marukame T, Ishikawa T, Matsuda K, Uemura T and Arita M *J. Phys. D:Appl. Phys.* 39 824 (2006) .
12. Kämmerer S, Thomas A, **Hütten A and Reiss G** *Appl. Phys. Lett.* 85 79 (2004) .
13. Okamura S, Miyazaki A, Sugimoto S, **Tezuka N and Inomata K** *Appl. Phys. Lett.* 86 232503 (2005).
14. Sakuraba Y, Hattori M, Oogane M, Ando Y, Kato H, Sakuma A, **Miyazaki T and Kubota H** *Appl. Phys. Lett.* 88 192508 (2006).
15. Sakuraba Y, Miyakoshi T, Oogane M, Ando Y, Sakuma A, **Miyazaki T and Kubota H** *Appl. Phys. Lett.* 89 0528508 (2006).
16. Oogane M, Sakuraba Y, Nakata J, Kubota H, Ando Y, *Sakuma A and Miyazaki T* *J. Phys. D: Appl. Phys.* 39 834 (2006).
17. Tezuka N, Ikeda N, Miyazaki A, Sugimoto S, **Kikuchi M and Inomata K** *Appl. Phys. Lett.* 89 112514 (2006).
18. Dunlap, R., **Effects of composition on the properties of magnetic shape memory alloys**, Halifax, Nova Scotia, March (2007).
19. Hem Chandra Kandpal, Vadim Ksenofontov, Marek Wojcik, **Ram Seshadri**, and **Claudia Felser**, *Electronic structure, magnetism, and disorder in the Heusler compound Co<sub>2</sub>TiSn*, *Journal of Physics D: Applied Physics*(2006).

20. Jepsen O and Andersen O K **Stuttgart tb-lmto-asa program version 47** <http://www.fkf.mpg.de/andersen/>, (2000).
21. **Ebert H The Munich spr-kr package**, version 3.6, <http://olymp.cup.uni-muenchen.de/ak/ebert/sprkr> ,(2005) .
22. Blaha, P. Schwarz, k., Madsen,G., Kvasnicka ,D.,& Luitz,J.2016. **WIEN2k An Augmented PlaneWavePlus Local Orbitals Program for Calculating Crystal Properties. In User's Guide.** Place Published: Vienna University of Technology (Release 12/12/2016).
23. Savrasov S Y and Savrasov D Y Phys. Rev. B 46 12181(1992).
24. A. Birsan, V. Kuncser, **Theoretical investigations of electronic structure and magnetism in Zr<sub>2</sub>CoSn full-Heusler compound**,arXiv:14117154v1[cond-mat.mtrl-sci]26Nov (2014).
25. A. Birsan, Magnetism in the new full-Heusler compound, Zr<sub>2</sub>CoAl: A **first-principles study**, Current Applied Physics 14 1434e1436 (2014).
26. X.T. Wang, J.W. Lu, H. Rozale, X.F. Liu, Y.T. Gui, G.D. Liu , **Half-metallic state and magnetic properties versus the lattice constant in Zr<sub>2</sub>RhZ (Z = Al, Ga, In) Heusler alloys**, School of Material Sciences and Engineering, Hebei University of Technology, 8 DingZiGu 1st Road, Tianjin, PR China (2015).
27. M.C. Payne, M.P. Teter, D.C. Allan, T.A. Arias, J.D. **Joannopoulos**, Reviews of Modern Physics 64 1065 (1992).

28. M.D. Segall, P.L.D. Lindan, M.J. Probert, C.J. Pickard, P.J. Hasnip, *S.J. Clark, M.C. Payne, Journal of Physics: Condensed Matter* 14 2717(2002).
29. Rakesh Jain, N. Lakshmi, Vivek Kumar Jain, Vishal Jain, Aarti R Chandra and K. Venugopalan, *Electronic Structure, Magnetic and Optical properties of  $Co_2TiZ$  (Z=B, Al, Ga, In)*, *Journal of Magnetism and Magnetic Materials* (2017).
30. Xiao-Ping Wei, Weiwei Sun, Ya-Ling Zhang, Xiao-Wei Sun, Ting Song, Ting Wang, Jia-Liang Zhang, Hao Su, Jian-Bo Deng, Xing-Feng Zhu, *Investigations on electronic, Fermi surface, Curie temperature and optical properties of  $Zr_2CoAl$* , *Journal of Solid State Chemistry* 247 97 (2017).
31. K. Koepernik, H. Eschrig, *Phys. Rev. B* 59 1743 (1999).
32. I. Opahle, K. Koepernik, H. Eschrig, *Phys. Rev. B* 60 14035 (1999).
33. Perdew J P, Burke S and Ernzerh of M *Phys. Rev. Lett* 77 3865 (1996).
34. H. J. Monkhorst, I. D. Pack, *Phys. Rev. B* 13 5188 (1976).
35. M. Jamal, IRelast Package is provided by M. Jamal as part of the commercial code WIEN2k. Available from: <http://www.wien2k.at/reg.user/unsupported/>; (2014).
36. F. D. Murnaghan, *proe. Natl. Acad. Sci. U.S.A.* 30 244 (1944).

37. Galanakis I. , Dederichs P. H. , Papanikolaou N. , **Slater-Pauling behavior and origin of the half-metallicity of the full-Heusler alloys**, Phys. Rev. B, 66 1744 29 (2002) .
38. Z. W. Huang, Y. H. Zhao, H. Hou, and P. D. Han, **Physica B** 407 1075 (2012) .
39. M. Born and K. Huang (Oxford; Clarendon) (1956).
40. Reuss, Z. Angew. **Math.** Mech. 9 49 (1929).
41. D. M. Teter, **MRS Bull.** 23 22 (1998).
42. S. Pugh , London , Edinburgh , *Dublin Philosophical Magazine*, **J Sci** 45 823 (1954).
43. C. Zener, **Elasticity and Anelasticity of Metals**, University of Chicago Press, Chicago (1948).
44. P. Ravindran, L. Fast, P. A. Korzhavyi, and B. Johansson, J. Appl. Phys. 84 4891 (1998).

جامعة النجاح الوطنية

كلية الدراسات العليا

الخصائص التركيبية والالكترونية والمغناطيسية والمرونية  
لمركبات هزلة الطبيعية والمعكوسة:  $Co_2TiSn$  &  $Zr_2TiSn$   
باستخدام الجهد التام

إعداد

ضحى نصر محمد أبو بكر

إشراف

أ.د. محمد أبو جعفر

قدمت هذه الأطروحة استكمالاً لمتطلبات الحصول على درجة الماجستير في الفيزياء، بكلية الدراسات العليا، في جامعة النجاح الوطنية، نابلس - فلسطين.

2018

## الخصائص التركيبية والالكترونية والمغناطيسية والمرونية لمركبات هزلر الطبيعية

والمعكوسة:  $\text{Co}_2\text{TiSn}$  &  $\text{Zr}_2\text{TiSn}$  باستخدام الجهد التام

اعداد

ضحى نصر أبو بكر

اشراف

أ.د. محمد أبو جعفر

### الملخص

تم فحص الخصائص التركيبية والالكترونية والمغناطيسية والمرونية لمركبات هزلر الطبيعية المعكوسة ( $\text{Co}_2\text{TiSn}$  &  $\text{Zr}_2\text{TiSn}$ ) عن طريق استخدام الجهد النظرية الكثافة الوظيفية (DFT) والجهد التام المزيد ذو الموجات المستوية الخطية (FP-LAPW) والتقريب التدريجي المعمم (PBE-GGA) ضمن اطار برنامج WIEN2k.

تم استخدام التقريب التدريجي المعمم (GGA) لحساب ثابت الشبكة (a) ومعامل الصلابة (B) ومشتقة معامل الصلابة بالنسبة للضغط (B') وأيضا تم استخدام نظام بيكي جونسون لتحسين فجوة الطاقة.

من أهم نتائج هذه الدراسة:

1. تبين أن المركبين  $\text{Zr}_2\text{RhGa}$  الطبيعي و  $\text{Co}_2\text{TiSn}$  العكسي يمتلكان الخاصية المعدنية.
2. تبين أن المركبين  $\text{Zr}_2\text{RhGa}$  العكسي و  $\text{Co}_2\text{TiSn}$  الطبيعي يمتلكان خاصية النصف معدنية.
3. تبين أن المركبات  $\text{Zr}_2\text{RhGa}$  العكسي و  $\text{Co}_2\text{TiSn}$  العكسي والطبيعي ذات خصائص مغناطيسية.
4. تبين ان النتائج التي اوجدناها قريبة من النتائج العملية والنظرية الاخرى.
5. من خلال خاصية المرونة أن المركبين  $\text{Zr}_2\text{RhGa}$  العكسي و  $\text{Co}_2\text{TiSn}$  الطبيعي مستقران ميكانيكيا.

ج

6. تبين أن مركب  $Zr_2RhGa$  العكسي قابل للسحب والطرق ومركب  $Co_2TiSn$  الطبيعي هش للانكسار.

7. تبين أن المركبين  $Zr_2RhGa$  العكسي و  $Co_2TiSn$  الطبيعي يمتلكان روابط أيونية.